**Universidade de Aveiro**

**2010**

Departamento de engenharia cerâmica e do vidro

**Zhonghua Wang**

# Cerâmicos e Filmes espessos de $Cu_3TeO_6$ : Fabricação e Caracterização

# $Cu_3TeO_6$ Ceramics and Thick Films: Fabrication and Characterization

**Universidade de Aveiro**

**2010**

Departamento de engenharia cerâmica e do vidro

**Zhonghua Wang**

# Cerâmicos e Filmes espessos de $Cu_3TeO_6$ : Fabricação e Caracterização

# $Cu_3TeO_6$ Ceramics and Thick Films: Fabrication and Characterization

Dissertação apresentada à Universidade de Aveiro para cumprimento dos requisitos necessários à obtenção do grau de Mestre em Ciencia e Engenharia dos Materiais (EMMS), realizada sob a orientação científica da Prof. Dr. Paula Maria Vilarinho, Professora Associada do Departamento de Engenharia Cerâmica e do Vidro da Universidade de Aveiro

## The Board of Examiners

President

Prof. Dr Maria Margarida Tavares Lopes De Almeida
Assistant professor of University of Aveiro

Prof. Dr Mário António Caixeiro De Castro Pereiraecided
Associate professor from University of Minho

Prof. Dr Paula Maria Lousada Silverinha Vilarinho
Associate professor of University of Aveiro

**Acknowledgement**

First of all, I would like to express the sincerest gratitude to my supervisor Prof. Dr. Paula M. Vilarinho for her patient guidance, meaningful discussions and precious suggestions for the thesis work, from which I have benefited tremendously. The research and study experience will surely be life-long treasures for me.

My thanks also go to all the awesome members in the Group of Electroceramics, University of Aveiro. Xinming, Amit, Monika, Sebastian, Asif and Sudheendran provided generous and substantial help with my experiments. I would like to thank the technicians in Department of Ceramics and Glass Engineering as well for their assistance.

I am grateful to my friends Randy and Joy Wades, Elizabeth and Armenio Anjos, Mary Ditmars. They have always been there and ready to give me encouragement, during the difficult times of my life.

I also want to thank the EMMS coordinators from University of Aveiro, Technical University of Hamburg-Harburg and Aalborg University for their hard work. I am indebted to the European Union for the financial support, without which my study in Europe would not have been possible.

To my parents and beloved wife Wenjing, all I want to say is "Wo ai ni men!". Their unreserved and endless love is the source of my strength.

**palavras-chave** A baixa temperatura de sinterização, LTCC, cobre tellurate, filmes espessos, depostion eletroforética, EPD

**resumo** Tem havido uma procura crescente de miniaturização nos dispositivos eletrônicos, mantendo a função de alta densidade e baixo preço. A solução definitiva é a cerâmica de baixa temperatura de co-incineração (LTCC) tecnologia. Segmentação LTCC aplicações, a fabricação e as propriedades dielétricas de $Cu_3TeO_6$ filmes espessos foram estudados nesta tese.

Os precursores foram sintetizados pelo método de reação no estado sólido convencional. Óxido de cobre (CuO) e dióxido de telúrio ($TeO_2$) pós como matérias-primas, com diferentes estequiometrias foram calcinados a uma série de temperaturas. Raios-X difração dos produtos e atestar que $CuTe_2O_5$ e $Cu_3TeO_6$ foram obtidos como os compostos mono-fásica para o $2CuO+TeO_2$ e composições $3CuO+TeO_2$, respectivamente.

Cerâmica $Cu_3TeO_6$ foram bem sinterizados a 865$^oC$, apresentando uma densidade relativa de 93% e retração de 29%. Sinterização a altas temperaturas levaram à decomposição de $Cu_3TeO_6$. A permissividade dielétrica da cerâmica aumenta com a temperatura de sinterização. A tangente de perda eo coeficiente de temperatura da permissividade dielétrica são muito elevados, que não cumpram os requisitos de materiais LTCC.

**Keywords** Low temperature sintering ceramics, LTCC, copper tellurate, thick films, electrophoretic depostion, EPD

**abstract**

There has been an ever-growing demand for miniaturization in the electronic devices while keeping the high function density and low price. The ultimate solution is the low temperature co-firing ceramics (LTCC) technology. Targeting LTCC applications, the fabrication and dielectric properties of $Cu_3TeO_6$ thick films were studied in this thesis.

The precursors were synthesized by the conventional solid state method. Copper oxide (CuO) and tellurium dioxide ($TeO_2$) powders as starting materials with different stoichiometry were calcined at a series of temperatures. X-ray diffraction analysis of the products attest that $CuTe_2O_5$ and $Cu_3TeO_6$ were obtained as mono-phasic compounds for the $CuO+2TeO_2$ and $3CuO+TeO_2$ compositions, respectively.

$Cu_3TeO_6$ ceramics were well sintered at 865$^oC$, showing a relative density of 93% and shrinkage of 29%. Sintering at higher temperature led to the decomposition of $Cu_3TeO_6$. The dielectric permittivity of the ceramics increased with the sintering temperature. The loss tangent and temperature coefficient of dielectric permittivity are very high, which do not meet the requirements of LTCC materials.

$Cu_3TeO_6$ green films were fabricated by electrophoretic deposition (EPD). The thickness of green film increased rapidly with deposition time in the initial stage. The electric field exhibited a linear relationship with the thickness at fixed time. However, the quality of the films deteriorated under high voltages (>300V). Sintering of the films was carried out from 800$^oC$ to 860$^oC$. The scanning electron microscopy (SEM) images of the film sintered at 860$^oC$ show a well densified microstructure. The $Cu_3TeO_6$ thick films exhibit poorer dielectric permittivity but lower loss tangent.

## List of Figures

# Table of contents

# *Chapter 1*

# Low sintering temperature ceramics

*"Because low-firing is the most basic of all ceramic techniques, it really treats all your senses."*

*--Sumi Von Dassow*[1]

## 1.1 Low sintering temperature ceramics: an introduction

The advances in electronics industry enabled the fabrication of individual components and entire functional units in the form of integrated circuits (IC), leading to the miniaturization of electronic devices.[2] However, the consumers have never ceased to demand for more compact products. A technical solution to this problem is the advanced packaging technique. More specifically, it is referred to as the simultaneous sintering of the conductor or insulator and substrates. In order to realize it, ceramics with low sintering temperatures are required.

In fact, low firing has been an everlasting topic in ceramics processing, owing to a series of benefits coming along with the decrease of the sintering temperature, such as energy conservation, reduced costs and improved properties.[3, 4] Moreover, ceramics, metallic and macromolecular materials have their unique electrical properties that have been combined in electronic devices and systems and thus requires a low temperature sintering of ceramics to make it compatible with metals and polymers.[5] Indeed a considerable amount of efforts have been committed to the development of ceramics with low sintering temperatures.

Generally, three approaches have been frequently used to lower the sintering temperature of ceramics: (1) the addition of glass or low melting oxides to the

ceramic matrix, such as $Bi_2O_3$, $B_2O_3$, and $V_2O_5$.[6, 7] This is the most popular method and has been intensively studied. Though the sintering temperature could be lowered, an obvious drawback exists due to the presence of the additives: the deterioration of the dielectric properties of the resultant materials. (2) Chemical processing of the raw materials by sol-gel, co-precipitation, among others, to reduce the particle size. However the procedures of chemical processing methods are often complicated and the cost is relatively higher as well. (3) Exploitation of new material systems with intrinsic low sintering temperatures.[8] The advantage of this method is the avoidance of using sintering additives and the reduction of the co-existing phases in the material.

The guideline for the material development aspect in this thesis work is based on the spirit of the third approach.

## 1.2 Applications of low sintering temperature ceramics

The ceramics with low sintering temperatures embrace a quite broad range of materials and applications. In the following part, some practical examples will be given on the applications of these materials, to unveil just the tip of an iceberg.

Lead zirconate titanate (PZT) is a piezoelectric material widely used in sensors, actuators and transducers.[9, 10] Sintering of PZT-based ceramics is normally carried out above 1200$^{o}$C in order to obtain the practical piezoelectric properties.[11, 12] Compositional control and the environment could suffer from the volatility of lead oxide at high temperatures. Moreover, the utilization of economical silver-based internal electrodes has recently been strongly demanded and thus imposed a strict requirement on fabricating multilayer piezoelectric devices at low temperatures. According to Hayashi et al.,[4] the addition of $LiBiO_2$ as sintering aid can considerably decrease the firing temperature and leads to the formation of a fully densified body of $Pb_{0.95}Ba_{0.05}\left[(Mg_{1/3}Nb_{2/3})_{0.125}\,\mathrm{Zr}_{0.445}\,Ti_{0.43}\right]O_3$ (PBMNZT) at low temperatures while the excellent piezoelectric properties are still maintained.

The electromechanical factor $K_p$ is 60.7% and the piezoelectric coefficient is approximately 467 pm/V for the ceramics sintered at 950$^{o}$C and with 0.7 wt.% $LiBiO_2$. These properties are sufficient for its application in actuator devices. Similar results were also reported by using 0.5 wt.% CuO+0.5 wt.% $Bi_2O_3$ as the sintering aids for the Sb, Li and Mn-substituted $Pb(Zr,Ti)O_3$-$Pb(Zr,Ti)_{1/3}Nb_{2/3}O_3$ ceramics.[13]

Solid oxide fuel cells (SOFCs) have attracted extensive attention due to the high energy conversion efficiency, low pollution emission and high flexibility to fuels. Electrolytes sintered at low temperatures are of practical importance to the SOFCs in reducing product cost.[14] Li and co-workers[15] fabricated fully dense ceria ceramics doped with 0-20 wt.% of samarium at 1000$^{o}$C by using the precursors synthesized through carbonate precipitation. The electrolytes synthesized at low temperatures have comparable electrical properties with those sintered at high temperatures.[16, 17] Low temperature sintering makes it possible for the electrolyte to be co-fired with other elements in the solid oxide fuel cells.

By far one of the most important applications of low sintering temperature ceramics is in the low temperature co-fired ceramics (LTCC) technology, an advanced multilayer packaging technology that allows the integration of the discrete surface mount passive components as well as the active components into the substrates to form a monolithic module.

## 1.3 Low temperature co-fired ceramics (LTCC) technology

### 1.3.1 Introduction to the LTCC technology

The low temperature co-fired ceramics (LTCC) technology was first developed by Hughes and DuPont® in the 1980s for applications in military systems and gradually extended to avionics and automotive areas, as well as the

multi-chip modules (MCMs) for communications and computer applications in the last twenty years.[18] Recently, the research on LTCC was dramatically pushed forward by the advancement of wireless communication systems, which is one of the most rapid growing divisions in the consumer electronic market. A series of products, such as mobile phones, global positioning systems (GPS) and wireless local area computer networks (WLANs) popped out as wireless communication products. These products, while facilitating the daily life of people, also laid in front of the researchers some substantial challenges, such as, light weight, compact size, reliable performance, high functional density and low price. A great number of efforts were dedicated to the research on advanced packaging technologies, which play an important role in satisfying the demand. Through the integrated circuit (IC) and other high-density packaging technologies, miniaturization of devices and improvement of the circuits were achieved to some extent. However, a majority of the passive elements, such as capacitors, resistors and inductors, are still discrete. Little improvement was made from the continuing reduction in the size of surface mounted components due to the incompatibility with the printed circuit board (PCB) technology.[19] Moreover, the assembly of the tiny discrete components is costly. In order to alleviate the aforementioned problems effectively, the solution has to meet these basic requirements: high reliability, low cost and the ability to embed both the active and surface-mount passive elements into the substrates and form a three dimensional multi-layer circuit board. As a result of the advantages it possesses over others, the LTCC technology stands out as the method of choice. Figure 1 shows the structure of a commercialized LTCC module (LFC® series, Murata manufacturing Co., Ltd.). Typically, it consists of a number of co-fired ceramic layers as substrates, passive components, connecting vias, external and internal electrodes, which are inter-connected by the three-dimensional circuitry.[20, 21]

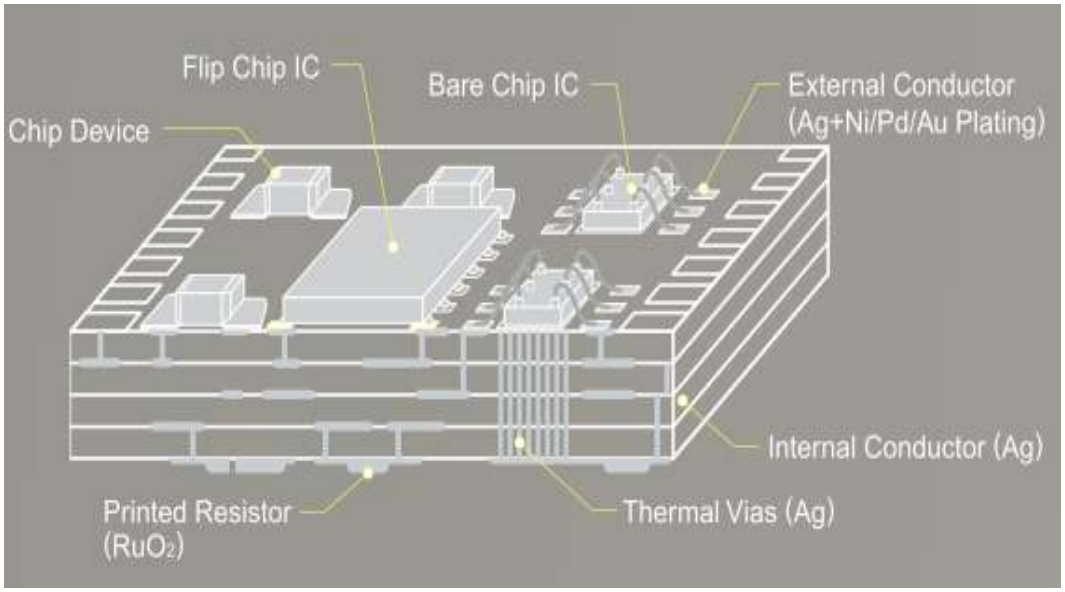


Figure 1. Schematic structure of a low temperature co-fired ceramic (LTCC) module (http://www.murata.com/products/catalog/pdf/n20e.pdf)

1.3.2 Fabrication process of LTCC technology

Figure 2 shows the manufacturing process for the LFC® series LTCC modules (Murata manufacturing Co. Ltd). The major steps involved in the fabrication process include:

(1) Green tape formation. The green films with a thickness of several tens of micrometers are fabricated by the tape casting method.[22]

(2) Blanking. The obtained green tapes are then cut into individual sheets and this is name as blanking.

(3) Via formation and filling. Vias are normally formed by a punching process and subsequently filled with the required materials, depending on the characteristics of the green tapes.

(4) Pattern printing. In this step, the conductor paste is screen-printed onto the green tapes to form the patterns.[23]

(5) Stacking and lamination. Stacking refers to the step that the green tapes are arranged in a proper order to form the multilayer structure. The

stacked tapes are then laminated by applying the heating and uniaxial pressing operations.

(6) Co-firing. The soft and flexible green tapes together with the embedded components are converted to a dense structure through the co-firing step. It is worth noting that the shrinkage variations in lateral directions of the films during the sintering process may cause reduced geometric precision, which consequently affects the application of LTCC technology in mass production of modules.

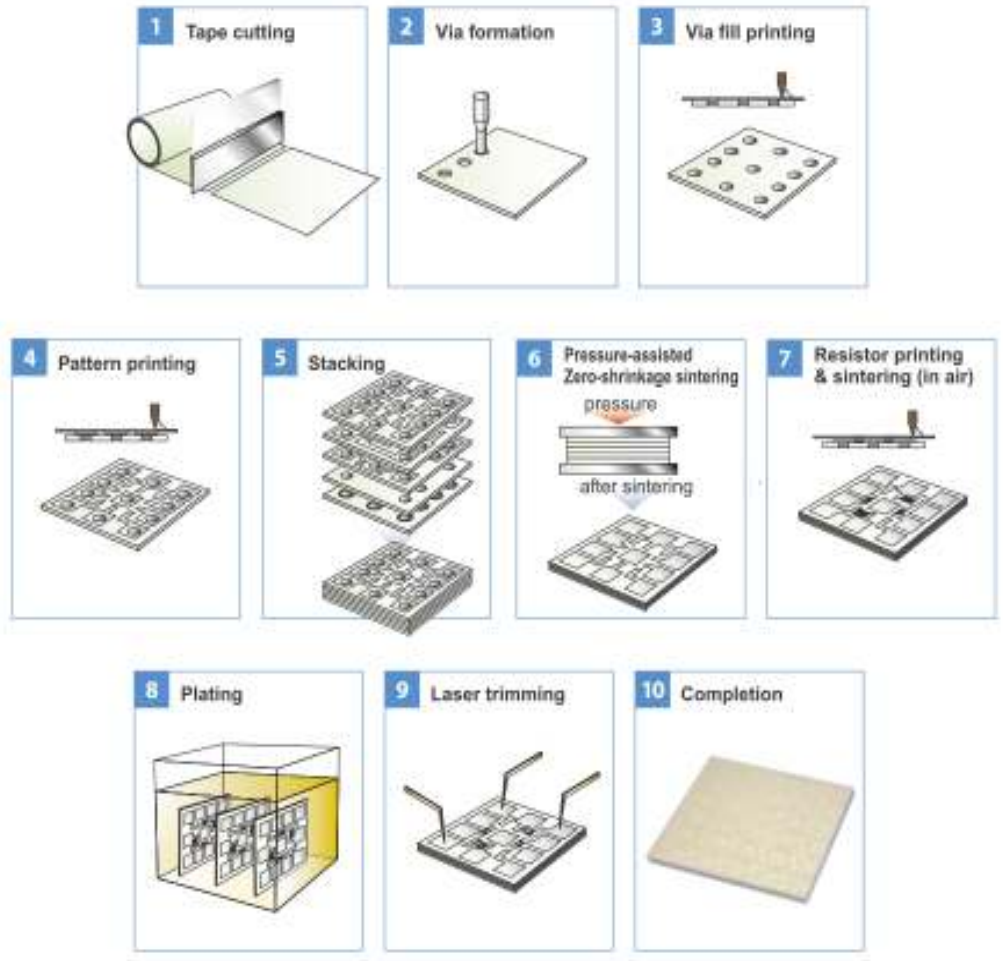


Figure 2. Schematic diagram of the LTCC manufacturing process (http://www.murata.com/products/catalog/pdf/n20e.pdf)

### 1.3.3 Material and application issues

The two characteristic features of the LTCC technology, as implied by its name, are “low temperature” and “co-fired ceramics”. The low temperature in the context of LTCC technology often refers to temperatures below 950$^{o}$C. This specific value was determined by the melting points of the inner electrode material silver, which has a melting point of 962$^{o}$C. In general, the noble metals, such as platinum, gold and silver, are the ideal candidates for the inner electrode materials in LTCC due to their high electric conductivity and low resistive loss at high frequency, which are crucial for the high-speed transmission of signal in the wireless communication systems. Taking into consideration cost issues, silver stands out as the most suitable material for inner electrodes. As a matter of fact, most of commercial LTCC modules in market use silver as the inner electrode material. Since the deterioration of the circuits and a loss of functionality will be caused by the melting of the inner electrode during the sintering process,[24] it should be strictly be avoided by keeping the processing temperature lower than the melting point of silver.

On one hand, the low temperature brings forth a series of benefits. On the other hand, to seek and develop appropriate compositions with low sintering temperatures, namely below 950$^{o}$C, is very challenging since most of the conventional ceramics are sintered at temperatures higher than 1200$^{o}$C.[25] Apart from the requirement on processing temperature, the LTCC materials should also have controlled dielectric permittivity ($\varepsilon_r$), high quality factor (Q) and near-zero temperature coefficient of resonant frequency.[26] The most widely used materials in the LTCC technology are the glass-ceramic composites. Commercialized LTCC materials, for instance, the green tapes supplied by Heraeus®, Murata®, DuPont® and Ferro®, are all based on the glass-ceramic compositions. Sebastian et al.[27] reviewed the dielectric materials applied in LTCC and gave a detailed list of various commercial glass-ceramics. As previously mentioned, the price of dielectric property deterioration may be paid for the

lowered sintering temperature of ceramics by the addition of glass phase, making it difficult to obtain very low dielectric loss in the LTCC modules.[21] Moreover, the possibility of chemical reactions with the metal electrodes are also promoted.[28] Therefore, a monophasic composition is favorable and can avoid the side effects caused by the glass additives.

Though most of its applications were found in the wireless communication systems, LTCC technology was used in many other areas to fabricate miniaturized devices, such as micropumps,[29, 30] pressure sensors[31] and spherical motors.[32] For instance, in the bio-medical device industry, LTCC technology was used to manufacture cavities and channels for drug delivery systems and automatic biological test modules, owing to its ability to build the three dimensional structures. Baker et al. [33] reported the fabrication of dielectrophoretic cell sorters using LTCC materials for contact-free alignment and trapping of suspended particles in the range of 10 μm. The device consists of two layers of electrodes separated by a 40 μm thick LTCC layer which forms the flow channels. Particles and cells are focused and trapped by the application of negative dielectrophoresis. Similarly, complex three-dimensional microfluidic structures with monolithic integration of thermal control, which can be applied in analytical chemistry, were also built by the LTCC technology.[34]

# *Chapter 2*

## Tellurium-based compositions

Tellurium dioxide ($TeO_2$) is well known as a glass network former and has a melting point of 733$^{o}$C. [35] The tellurite glasses exhibit high refractive index, high ionic and electric conductivity, good optical transmission in the infrared spectrum and low processing temperatures.[36] Due to the low melting temperature of tellurium dioxide, the tellurium-based ceramics, as potential candidates for the LTCC technology, have recently attracted increased research interests. However the information on this topic is still very scarce and only a few groups are working on it. Table 1. includes the main research groups and their contribution to different Te-based ceramics. It is worth noting that only the group from UA (Portugal) reported the Te-based thick films fabricated by electrophoretic deposition (EPD) for the microelectronic applications.[37]

Table 1. Some research groups and their work on tellurium-based ceramics

| Groups | Te ceramics | Time |
|---|---|---|
| Musashino Lab group (Nippon telegraph and telephone Public Corporation, Japan)[38] | $SrTeO_3$ | 1972 |
| Danilo Suvorov's group (Jožef Stefan Institute, Slovenia) | $CaTeO_3$, $CaTe_2O_5$, $TiTe_3O_8$, $Bi_2Te_2O_8$, $Bi_2TeO_6$, $Bi_6Te_2O_{15}$ | 2001 |
| Clive Randall's group (Penn. State University, USA) | $BaTe_4O_9$ , $Ba_2TeO_5$ | 2005 |
| Paula Vilarinho's group (University of Aveiro, Portugal) | $TiTe_3O_8$ (thick films) | 2009 |

## 2.1 $TiO_2$-$TeO_2$ system

In the $TiO_2$-$TeO_2$ binary system, $TiTe_3O_8$ was the only compound reported to be thermodynamically stable and could be synthesized at 700°C in air.[39] The crystal structure of $TiTe_3O_8$ is cubic (space group $I2_1/a\bar{3}$) with a unit cell parameter with a=10.965 Å.[40] The dielectric properties of $TiTe_3O_8$ ceramics at microwave frequency were first studied by Maeda at al.[41] The relative permittivity is 36 while the quality factor $(Q \times f)$ is 10200 GHz and the temperature coefficient of resonant frequency ($\tau_f$) -220 ppm/°C at 4GHz.

According to the research by Udovic et al.,[42] $TiTe_3O_8$ is obtained from the solid state reactions of titanium dioxide and tellurium dioxide regardless of the molar ratios of starting materials. The $TiTe_3O_8$ ceramics sintered at 720°C exhibit a dielectric permittivity ($\varepsilon_r$) of 50, a quality factor ($Q \times f$) of 30600 GHz and a temperature coefficient of resonant frequency ($\tau_f$) +133 ppm/°C at 5GHz. The dielectric properties of the ceramics are nearly independent of the processing parameters. And this is attributed to the low concentration of defects in the grains, as revealed by the transmission electron microscopy (TEM) studies. The addition of $TeO_2$, which is compatible with the $TiTe_3O_8$ main phase, to the binary system leads to a decrease of the sintering temperature and lowered the temperature coefficient of the resonant frequency. With the composition of $0.85TiTe_3O_8$ - 0.15 $TeO_2$, the ceramic sinters at 670°C and the resulted temperature coefficient of resonant frequency ($\tau_f$) reaches a near-zero value. The tunable dielectric properties at microwave frequency make the titanium tellurate ceramics very attractive in microelectronics.

## 2.2 $Bi_2O_3$-$TeO_2$ system

Bismuth-based dielectric ceramics have already been known for their relatively low sintering temperatures at around 1100°C since the 1990s.[43, 44] For a long time, the bismuth and tellurium oxides have been studied as glasses

and were applied in optical communication and photorefractive materials.[45] A phase diagram of the tellurium dioxide and bismuth oxide binary system (Figure 3) was reported by Kikushi et al.[46] In this diagram, however, only merely two stable compounds, $Bi_6Te_2O_{15}$ and $Bi_2Te_2O_7$ can be found.

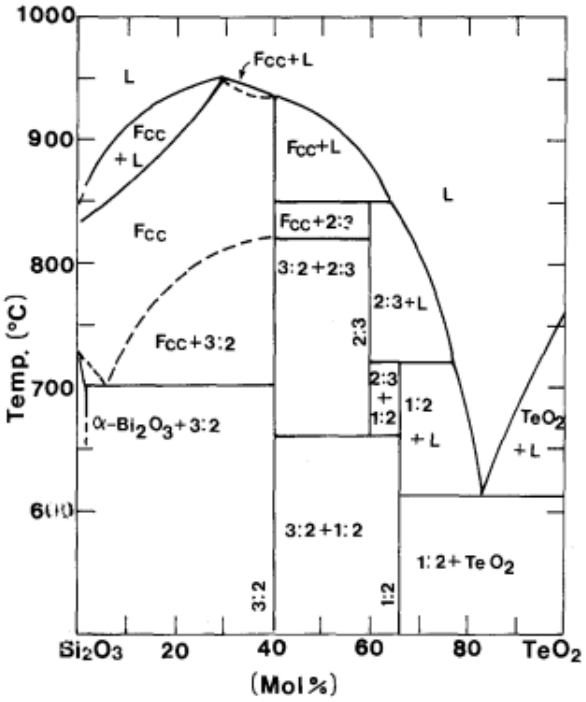


Figure 3. Phase diagram of the $Bi_2O_3$-$TeO_2$ binary system[46]

The investigation on the $Bi_2O_3$-$TeO_2$ system as ceramics for the microelectronic applications was carried out only recently by Udovic et al.[47] In oxygen atmosphere, four room-temperature stable compounds were synthesized by solid state reactions: $Bi_2Te_2O_8$, $Bi_2TeO_6$, $Bi_6Te_2O_{15}$ and a compound with a nominal composition of $7Bi_2O_3{\cdot}2TeO_2$. Dense ceramics fabricated from these four precursors sinter between 650°C and 800°C in an oxidizing atmosphere and their dielectric permittivity, $Q \times f$ value and temperature coefficient of resonant frequency ($\tau_f$) range from 30 to 54, 1.1 to 40.0 GHz (5GHz) and -43 to -144

ppm/$^{o}$C, respectively. It is worth noting that $Bi_6Te_2O_{15}$ and $7Bi_2O_3{\cdot}2TeO_2$ do not react with silver and could possibly be used in the LTCC technology.

### 2.3 ZnO-$TeO_2$ system

Like others in the tellurium oxide system, $Zn_2Te_3O_8$ composition was studied as a potential candidate for applications in LTCC as well.[48] The mono-phasic $Zn_2Te_3O_8$, having a monoclinic crystal structure, was synthesized by the calcination of stoichiometrically mixed ZnO and $TeO_2$ powders at 480$^{o}$C for 10 hours. Fully dense ceramics were obtained at 585$^{o}$C and the resultant dielectric permittivity is $\varepsilon_r$=16.7 while the quality factor and temperature coefficient of permittivity are $Q \times f$=66000 GHz and $\tau_f$=-60 ppm/$^{o}$C, respectively. The addition of 4 wt% $TiO_2$ improved the $\tau_f$ to -8.7 ppm/$^{o}$C. Moreover, the interaction with Ag was not observed in the scanning electronic microscopy (SEM) analysis of $Zn_2Te_3O_8$ ceramics.

### 2.4 CaO-$TeO_2$ system

Calcium tellurate ceramics were fabricated by Valant et al.[49] with a similar purpose as the previous studies, i.e. to evaluate their potential as low-permittivity substrate materials used for the LTCC technique. $CaTeO_3$ and $CaTe_2O_5$ were both obtained as single-phase compounds and the correspondent ceramics sinter at 840$^{o}$C and 780$^{o}$C, respectively. However, a fatal drawback of this tellurium-based system is the reactivity with silver, which is normally used as the inner electrode in the LTCC technology. For this reason, the calcium tellurates are ruled out from the LTCC application though they meet the requirement of low dielectric losses and low temperature sintering ceramics.

### 2.5 BaO-$TeO_2$ system

Based on the precedent works on the Te-based systems, it was supposed that a series of excellent dielectric ceramics with very low sintering temperatures could also be obtained from the BaO-$TeO_2$ system. In the work carried out by Kwon et al.,[50] four barium tellurates compounds were synthesized by the

conventional solid state reactions. $BaTe_4O_9$ and $Ba_2TeO_5$ were obtained as single phases after calcination at 500°C and 850°C in air, respectively. $BaTe_2O_6$ with $BaTe_2O_5$ and $BaTeO_3$ with $BaTeO_4$ as secondary phases were synthesized at 600°C and at 750°C, respectively. Dense ceramics of the aforementioned compositions were obtained by sintering the pressed pellets in air and the porosity was less than 2%. With the increment of barium content in the composition, the sintering temperature tends to increase.

The relative dielectric permittivity of the barium tellurates ceramics lie in the range of 10-21 at microwave frequency. A distinguished dielectric property of the ceramics, compared with that of the commercial glass-ceramic LTCC materials, is their very low dielectric loss at the microwave range. The temperature dependence of dielectric permittivity is very small and almost linear from -150°C to 150°C. Moreover, all of the temperature coefficients of dielectric permittivity ($TC\varepsilon_r$) for the ceramics in have positive values. However, the underlying mechanisms were not clear yet.[50]

If the temperature coefficients of dielectric permittivity ($TC\varepsilon_r$) could be adjusted to a near-zero value, the $BaO$-$TeO_2$ ceramics with their other advantages, such as low sintering temperatures, intermediate dielectric permittivity and low dielectric loss (i.e. high quality factor $Q \times f$) at microwave frequency, will attract more attention for the applications in the microelectronics industry.

### 2.6 $BaO$-$TiO_2$-$TeO_2$ ternary system

As mentioned above $TeO_2$-based binary and ternary systems have either large positive or negative temperature coefficient of resonant frequency ($\tau_f$) and thus it may restrict their applications in low temperature co-fired ceramics, where a near-zero temperature coefficient of resonant frequency is normally required. A possible approach to tune the temperature coefficient of resonant frequency of the binary system dielectrics, according to *Jiao et al*,[51] is through

the formation of a ternary system by sintering two single-phase end members of the phase diagram. In their research, $BaTe_4O_9$ and $TiTe_3O_8$ powders as end members were synthesized at 550°C and 840°C, respectively. Adjusting the ratios of powders, different compositions of $xBaTe_4O_9$-$(1-x)TiTe_3O_8$ (x=0.47, 0.50, 0.53, 0.57) dielectrics were obtained at sintering temperatures ranging from 520°C to 580°C. Both of the two single phases as well as a small amount of $BaTeO_3$ formed by decomposition were confirmed by the XRD analysis.

Electrical measurement data shows that the ceramic with the composition of $0.47BaTe_4O_9$-$0.53TiTe_3O_8$ has a relative permittivity of 28, a quality factor ($Q \times f$) of 12,200GHz at 10GHz and a temperature coefficient of resonant frequency value of 4 ppm/°C, making it a potential candidate for the LTCC application.[51] The reason for the ternary system having such a low temperature coefficient of resonant frequency is explained by the fact that the single-phase compositions $BaTe_4O_9$ and $TiTe_3O_8$ have positive and negative temperature coefficient of resonant frequency ($\tau_f$), respectively, and the two offset each other to a near-zero value at the proper mole ratio.

Kwon *at al*.[52] also reported the synthesis of a single-phase compound $BaTiTe_3O_9$ of the ternary system $BaO$-$TiO_2$-$TeO_2$ by using BaO and $TiTe_3O_8$ as starting materials. Fully densified $BaTiTe_3O_9$ ceramics were obtained at sintering temperatures ranging from 625°C to 650°C. $BaTiTe_3O_9$ ceramics have a medium dielectric permittivity but an exceptionally high negative temperature coefficient of resonant frequency ($\tau_f$=-337 ppm/°C) with respect to its relative permittivity.

Information about the commercialization of the above mentioned Te-based ceramics is not available yet. This might be attributed to the extreme rarity of the tellurium element,[53] which is comparable to that of platinum and thus multiplies the production costs.

## 2.7 Tellurium-based thick films

The dielectric properties of the tellurium-based compositions were briefly described only as bulk ceramics in the last paragraphs. But in fact, thick films of the tellurium-based compositions are of relevant importance for applications in microelectronics. Su *et al*.,[37] reported for the first time, the fabrication of titanium tellurite thick films through electrophoretic deposition (EPD) and the dielectric properties of the sintered thick films. Figure 4 shows the microstructure of the films and ceramics.

The green thick films were deposited onto a platinized silicon substrate and well sintered at 700$^{o}$C, which is 40$^{o}$C lower than sintering temperature of the correspondent bulk ceramics. The relative permittivity of sintered thick films is 54 while the dielectric loss is 0.009 at 100 KHz. The temperature coefficient of permittivity is +78 ppm/$^{o}$C.[37] The above mentioned properties make the thick films possible candidates in the integrated capacitors and microwave applications.

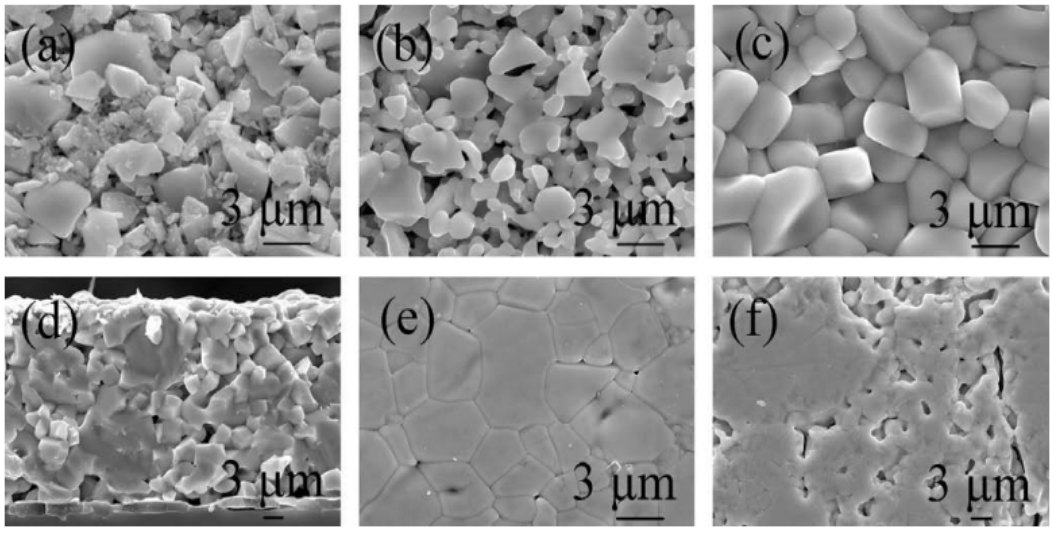


Figure 4. Scanning electron microscopy (SEM) images of $TiTe_3O_8$ films and ceramics. Plan view images of a green film (a) films sintered at 640$^{o}$C (b) and

700$^{o}$C (c) for 5 hours. Cross section images of a film sintered at and 700$^{o}$C for 5h (d). Polished surface of a ceramic sintered at 700$^{o}$C for 5h (e and f).[37]

## 2.8 $CuO$-$TeO_2$ system

Research and relevant data on the compounds of $CuO$-$TeO_2$ system are rather scarce and most of these limited research interests were targeted on the structural, optical and electrical properties of copper tellurium oxide glasses.[54] Early studies of this system mainly focused on the determination of the crystallographic structures of the compounds. So far, three compounds of the $CuO$-$TeO_2$ binary system have been obtained from the solid-state reactions and resolved for their crystal structures ($Cu_3TeO_6$, $CuTe_2O_5$, $CuTeO_3$). Hostachy *et al.*[55] and Falk *et al.*[56] calculated the crystallographic parameters from the XRD analysis data of $Cu_3TeO_6$ powders and single crystals, showing that $Cu_3TeO_6$ has a cubic structure (*Ia3*), which is built up by the $TeO_6$ octahedra connected through copper atoms. Lindqvist[57] and Hanke *et al.*[58] determined the crystal structure of $CuTe_2O_5$, which was synthesized as single crystals based on the method described by Moret *et al.*[59] $CuTe_2O_5$ crystalizes within the space group $P2_1/C$ and its unit cell parameters are: a=6.871Å, b=9.322Å, c=7.602Å and β=109.08$^{o}$. The structure is a three dimensional network formed by copper and tellurium polyhedra sharing oxygen atoms (Figure 6). In the $CuTeO_3$ structure (orthorhombic, *Pmnb*) two chemically different tellurium atoms exist and they are linked with copper atoms by the oxygen.[57, 60] The coordination of copper and tellurium atoms is shown in Figure 7.

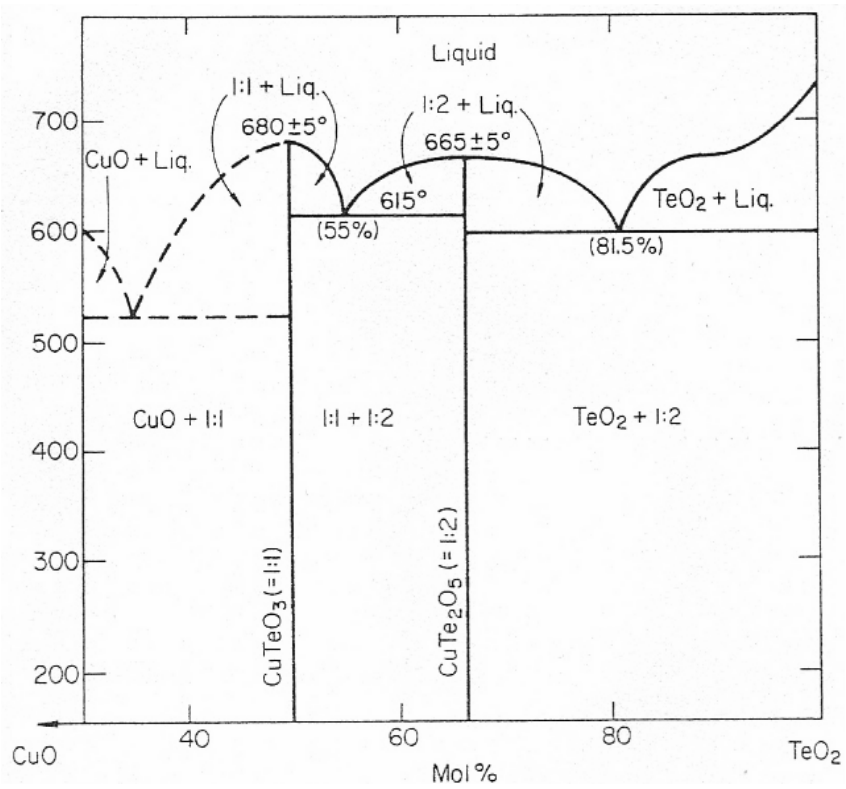


Figure 5. Phase diagram of the CuO-$TeO_2$ system[61]

Later on, three binary copper tellurates compounds obtained by wet-chemistry processing, $CuTeO_4$, $Cu_3TeO_6$ and $CuTeO_3$, were reported by Gospodinov,[62] being synthesized at the temperatures of 267-470$^oC$, 595$^oC$ and 840-880$^oC$, respectively. The reactions were carried out via the in-air thermolysis of copper hydrogen tellurate ($CuH_4TeO_6$), which was prepared by the precipitation reaction of the aqueous solutions of $CuSO_4$ and $Na_2H_4TeO_6$ in the presence of alkaline base. [62]

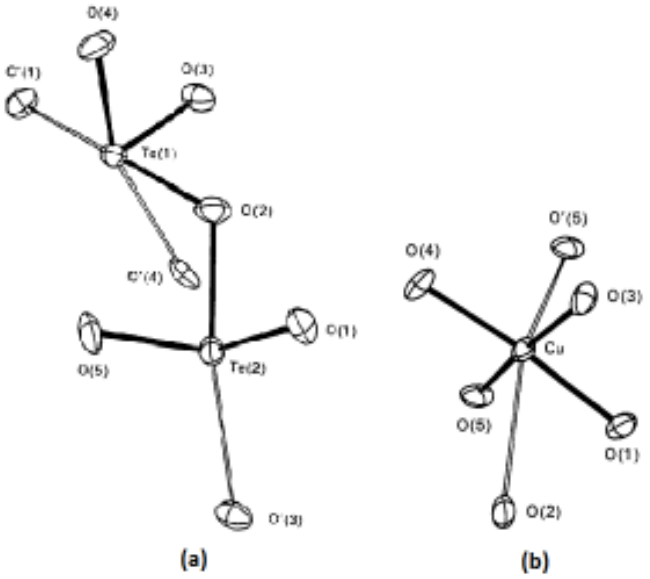


Figure 6. Coordination of Te (a) and Cu (b) in $CuTe_2O_5$[58]

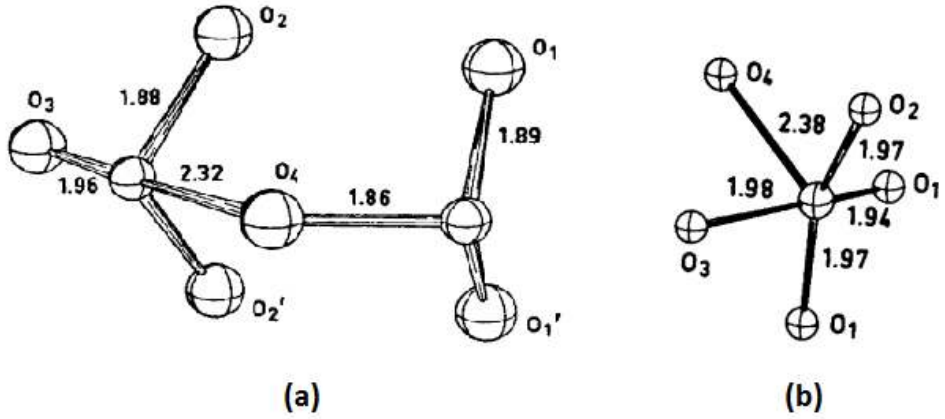


Figure 7. Coordination of Te (a) and Cu (b) in $CuTeO_3$[60]

In conclusion, some compounds based on copper oxide and tellurium dioxide were obtained through various approaches. However, their study was merely limited to the glasses. In addition, the fabrication of CuO-$TeO_2$ ceramics and films and the investigation of their physical electrical properties have not been reported yet. Therefore and due to the quite low synthesis temperature of these

compounds the fabrication of both bulk ceramics and thick films of copper tellurium oxides and the characterization of their dielectric response is of high interest in view of their possible applications and contribution impact it may have to the advancement of LTCC technology.

# *Chapter 3*

# Electrophoretic Deposition (EPD): Introduction and applications to the fabrication of thick films

The demand for miniaturization of the electronic products has been driving thin and/or thick films of dielectric materials to replace the dielectric components presently in use in the form of bulk ceramics.[63] Materials in the form of films are of technological importance due to their easy miniaturization, high reliability and low driving voltages. Depending on their thicknesses, films basically fall into two categories: thin film (<1μm) and thick films (1μm-100μm). In fact, thick films, rather than thin films, are more favorable for the applications in the electronic as these are the volume devices that store the electromagnetic energy within the dielectric volume.[64]

A considerable amount of research has been dedicated to film fabrication techniques, which can be divided into two general classes: physical vapor deposition (PVD) and chemical deposition techniques, including chemical vapor deposition (CVD) and chemical solution deposition (CSD).[65] Generally Thin films can be obtained by sol-gel processing, molecular beam epitaxy, magnetron sputtering, pulsed laser deposition (PLD), physical vapor deposition (PVD), metal-organic chemical vapor deposition (CVD) and so on.[66] These methods, however, are not applicable for thick films fabrication due to the slow deposition rates and the accumulated stresses that may cause cracking of the thick films. For example, it is very difficult obtain films thicker than 1 μm by the conventional sol-gel method and the probability of getting defect films increases with the film thickness increase.[67]

The thick film technology was introduced into the electronic industry in the 1960s as a method to implement the hybrids packages with thick films.[68] Since then, a number of techniques have been used to form thick films upon the substrates. In the following parts, a brief introduction will be given to the most common thick film fabrication techniques, such as tape casting, screen printing, ink-jet printing and electrophoretic deposition (EPD).

Table 2 thin and thick films deposition techniques[65]

| **Thin Film Techniques** | **Thick Film Techniques** |
|---|---|
| *Physical vapor deposition* | Tape casting |
| Sputtering (rf magnetron, dc, ion beam) | Screen printing |
| Evaporation (e-beam, resistance, molecular beam epitaxy) | Electrophoretic deposition |
| Laser ablation | Hybrid sol-gel technique |
| *Chemical deposition* | |
| *Chemical vapor deposition* | |
| MOCVD (metal-organic CVD) | |
| PECVD (Plasma-enhanced CVD) | |
| LPCVD (Low pressure CVD) | |
| *Chemical solution deposition* | |
| Sol-gel (solution gelation) | |
| MOD (metallorganic deposition) | |

## 3.1 Thick films processing technologies

### 3.1.1 Screen printing

Screen printing is the most widely used thick film fabrication technique that allows a full two dimensional patterning of the films. As illustrated in Figure 8, the green films are obtained as the squeegee forces the ink in front of it through the open area of the screen and onto the substrates.[69] Direct patterning of the films is the most significant advantage of the screen printing technique over the others. The resolution of the pattern is co-determined by the mesh size and the rheological properties of the ink.[70] Theoretically, the thickness of the green films is determined by the volume of the ink forced through the screen, which is a function of the applied force on squeegee, the snap-off distance, the speed of the squeegee and the rheological properties of the ink.[69]

In the environmental monitoring application, screen printing was used to fabricate gas sensors, due to its good reproducibility and low costs.[71, 72] Martinelli *et al.* reported that screen printed thick films of Perovskite-type $LaFeO_3$ and $SmFeO_3$ on alumina substrates exhibit good agreement with the conventional instrument in test results and can be used to detect oxidizing gases.[73]

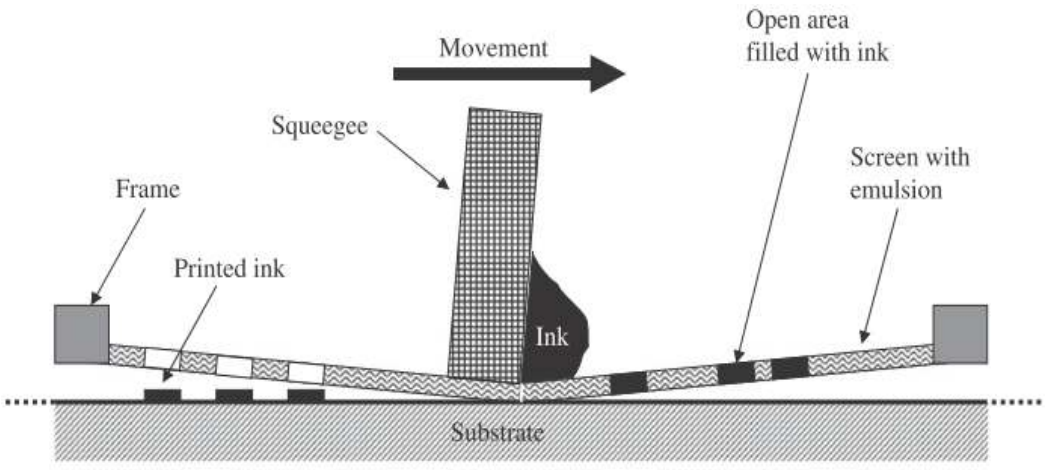


Figure 8. Schematic of screen printing process [74]

3.1.2 Tape casting

Tape casting, mainly used in the electronics industry, is a well-established technique for the fabrication of thick films in a large scale.[75, 76] Originally this method was developed to form piezoelectric thin sheets and produce multi-layer capacitors in the 1940s.[77] An advantageous feature of tape casting is attributed to its ability to produce many layers of green tapes which may have different compositions. The many layers can be deposited to form, by heat, pressure or dwell time, a monolithic structure.

In the tape casting process, a sharp blade is fixed above the substrate at a certain distance. The slurry, which consists of ceramic powders, solvent, dispersant, plasticizer and binder, is placed in front of the blade and cast onto a stationary or moving surface to form the green films. A doctor-blade set-up for the tape casting process is schematically shown in Figure 9.[68] The thickness of the green tapes is determined by the distance between the blade and the substrate, the surface energy of the substrate, the viscosity and surface energy of the slurry. After drying, the thickness of the films can be predicted by the empirical relationship[74]

$$d = \frac{1}{2}(g\frac{c}{\rho})$$

where $g$ stands for the distance between the blade and the substrate, $c$ for the concentration of the ceramic particles in the slurry in g/cm$^3$ and ρ for the density of the dried film in g/cm$^3$. Generally, the films produced by tape casting have a typical thickness of 100 μm to 300 μm.

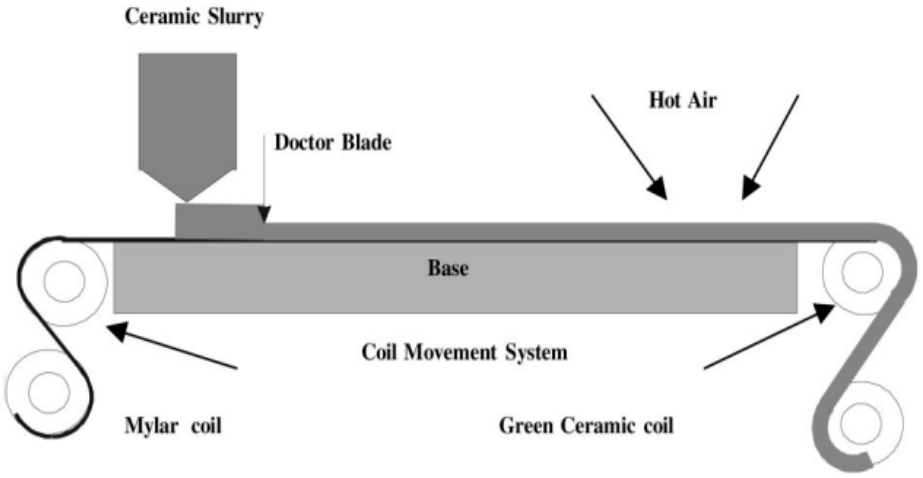


Figure 9. Schematic of tape casting process[68]

With fixed instrumental conditions, the most important parameter to control in the tape casting process are those related with the slurry properties. Appropriate rheological properties and high solid content and pseudoplastic behaviors could grant the green films high uniformity and high green density without segregation of the binder. The drying behaviors of the slurry affected the drying speed of the green films and the obtained thickness. Traditionally, organic solvents were used as the liquid medium to prepare the slurry. In recent years, with the accumulating concerns over the organic solvents' toxicity to human health and contaminations to the environment, research efforts were diverted to the aqueous tape casting.[78, 79]

3.1.3 Jet printing

Jet printing is a versatile process which has been applied in the fabrication of organic transistors, light-emitting diode, ceramic thick films and biopolymer arrays.[80] A jet printing process involves the spraying of the ink as individual droplets on the substrates to form a continuous coating or layer by keeping the droplet either separated or slightly overlapped.[81] Figure 10 schematically shows an apparatus used for the jet printing. Normally, low viscosity and relatively high surface tension of the inks are required for the jet printing process. The properties of the fabricated thick films can be controlled through the variation of the chemical and physical properties of the inks.

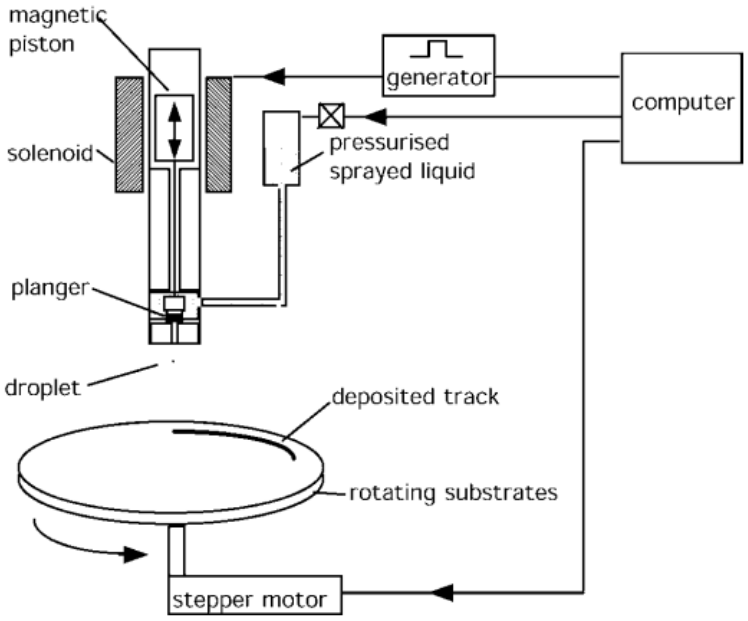


Figure 10. Schematic diagram of the jet printing apparatus[80]

## 3.2 Electrophoretic deposition (EPD)

3.2.1 Introduction

Electrophoretic deposition (EPD) is defined as a colloidal processing technique that can deposit charged particles onto a substrate to form coatings or films directly from a suspension.[82] The discovery of electrophoresis

phenomenon can be traced back to the early 1800s when the Russian scientist Ruess observed the movement of clay particles in water caused by the electric field. However, the practical application of EPD did not appear until 1933, with the deposition of thoria particles on a platinum cathode as emitter for an electron tube when it was patented in USA.[83]

In the EPD process, the solid particles are well dispersed in the liquid medium and with the optimal surface charge as a result of the electrochemical equilibrium with the solvent. When an external electric field is applied, the charged particles move toward the substrates that have opposite charge and a rigid deposition of particles happens forming a rigid layer on the top of that surface / substrate (Figure 11).[84] A post-EPD heat treatment is normally required to convert the loosely packed deposits into dense layers.

Depending on the sign of the surface charge of the particles, electrophoretic deposition is further divided into anodic and cathodic EPD. If the particles are positively charged, the deposition will take place on the cathode and the process is called cathodic EPD. Similarly, the negatively charged particles lead to anodic deposition.[85]

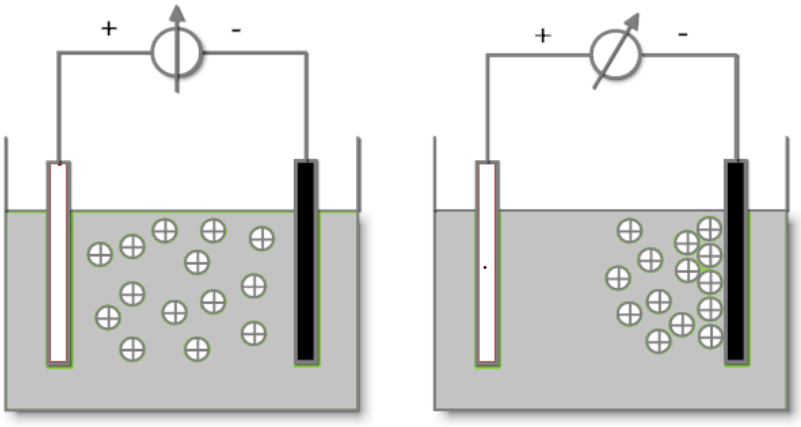


Figure 11. Schematic of EPD process

The EPD technique has many advantages over other film fabrication techniques. First of all, the apparatus used in EPD, as shown in Figure 12, is rather simple and easily accessible. A DC power supplier, two electrodes and a suspension container are all the basic components that are needed to assemble a set of EPD apparatus. Besides, there is no restricted requirement on the shapes of the substrates used for deposition, which makes the EPD technique unique and very suitable for versatile applications. Short processing time and thus low cost make it an attractive solution for industrial applications from the economical point of view. As a result, the EPD technique has found its applications in solid oxide fuel cells (SOFC),[86, 87] anti-oxidant coating, wear resistant coating and multi-layer composite material fabrication as well.[88]

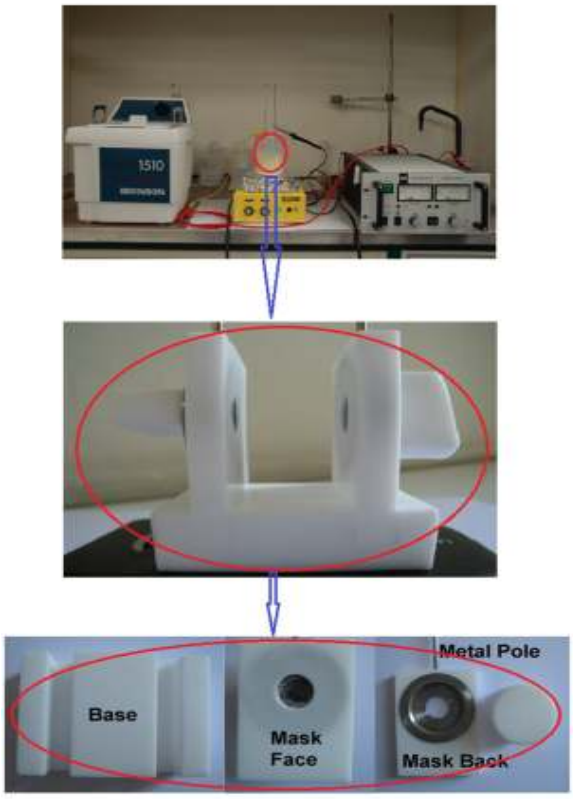


Figure 12. Set-up of the EPD device

### 3.2.2 Suspension stabilization

It is well recognized that obtaining a stabilized, unagglomerated and homogeneous suspension is critical to the quality of films fabricated by EPD. Stabilization of the suspensions can be achieved if the particles have high zeta-potential while keeping the ionic conductivity low. A necessary but not sufficient condition for the high zeta-potential is a high surface charge.[89] In general, the surface charge can be developed from the following processes: (i) dissociation or ionization of the surface groups on the particles. This is commonly observed with carboxylic acid, amine and oxide surfaces. The charge, in this case, is dependent on the pH value of the suspension; (ii) selective adsorption of ions onto the particle surface from the liquid medium. For example, in the AgI-water system, either the $Ag^-$ or $I^-$ ions adsorb on the surface of the particles; (iii) adsorption of ionized surfactants. Carbon black obtains negative surface charge by adsorption of anionic surfactant; (iv) isomorphic substitution. In Kaolinite, the $Si^{4+}$ is substituted by the $Al^{3+}$, resulting in negative charge.[82] In the non-aqueous medium, however, it is proved that the surface charge can be obtained only by the ionization of surface groups and the adsorption of ionized surfactants.[90]

Compared with those used in other colloidal processing techniques, EPD suspensions have a much lower solid loading, in order to keep a low viscosity. In the suspension, the surface-charged particles are surrounded by the counter ions at a concentration higher than that in the bulk liquid medium. This ionic atmosphere is called “electrical double layer”. A part of the counter ions are attracted to the particle surface to form the “Stern layer” and the rest are distributed in the “diffuse layer” or “lyosphere”. The potential established between the surface of the Stern layer and the diffuse layer is “zeta potential”, as shown in Figure 13. The overlapping of the diffuse layers determines the interaction between the particles.[82]

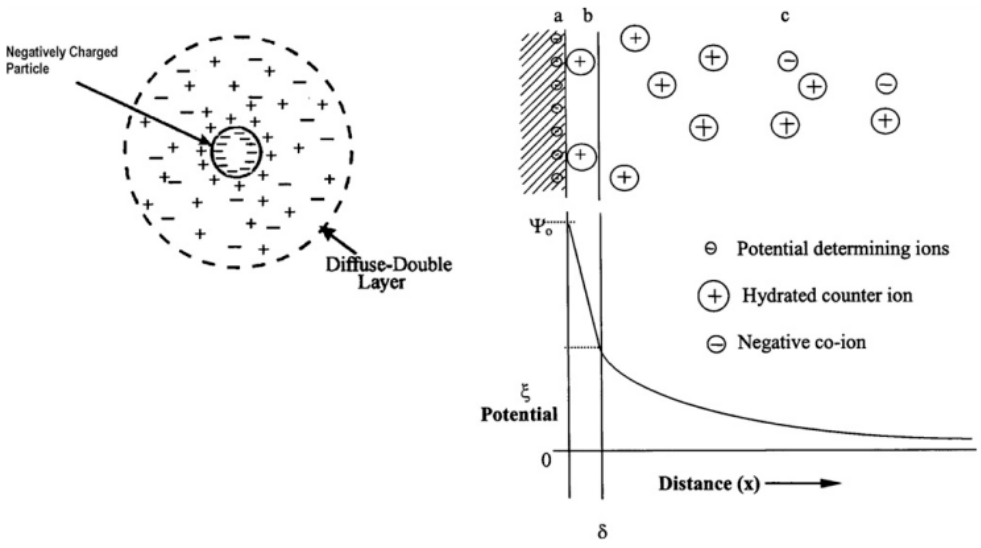


Figure 13. Schematic of the electric double layer and the zeta potential

(a) particle surface (b) Stern layer (c) diffuse layer

The interaction between the particles involves two forces: the repulsive electrostatic force, which results from the overlap of the diffuse layers and the attractive Van der Waals force. The stability of the suspension is dependent on the overall effect of these two forces. A quantitative description of the stability of the suspension in terms of energies of interactions between the colloidal particles is best presented by the DLVO theory (Derjaguin-Landau-Verwey-Overbeek). With the assumption that the attractive and repulsive forces are additive, the total energy of interaction can be expressed as a sum of the two,

$$V_{total}=V_a+V_r$$

where Va and Vr refers to the attractive and repulsive forces, respectively. Since the repulsive van der Waals interaction is not sensitive to the suspension properties, it is more effective to control the interaction by changing the repulsive forces, which in turn relies on the zeta potential. Adjust the zeta potential to a higher value so that the electrostatic force can suppress the attractive van der Waals forces and particles are kept apart from one another.

### 3.2.3 Influencing factors in the deposition process

The factors that have influence on the electrophoretic deposition are either related to the operation parameters, such as applied voltage and deposition time, or the intrinsic properties of the suspension, including viscosity, solid concentration, zeta potential and so on. Many efforts were committed to correlate these parameters with the amount and quality of the deposit. According to Ishihara et al.,[91] the mass of deposited particles upon the substrate at the initial stage can be determined by the equation below:

$$w = \frac{2}{3} C \cdot \varepsilon_0 \cdot \varepsilon_r \cdot \xi \cdot \left(\frac{1}{\eta}\right) \cdot \left(\frac{E}{L}\right) \cdot t$$

where C stands for the concentration of the particles, $\varepsilon_0$ for the permittivity of vacuum, $\varepsilon_r$ for the relative permittivity of the solvent, $\xi$ for the zeta potential of the particles, $\eta$ for the viscosity of the solvent, *E* for the applied voltage, *L* for the distance between the electrodes and t for the deposition time. Among these parameters, *E* and *t* are the variable factors during the deposition process while others are determined by the device and suspension. In the follow sections the influences of applied voltage and deposition time are discussed.

(i) *Applied voltage*. In general, increasing the voltage leads to higher deposition rate and thus a larger amount of deposit in a given time. However, the quality of the obtained films deteriorates when the voltage becomes too high. As the electrophoretic deposition is a kinetic process, the packing of the particles onto the substrate need time to reach the optimized state. If the electric field intensity is too high, the particles may move too fast, create turbulence in the suspension and make difficult to find suitable positions to form the required close-packed structure. In the meantime, the particles with larger size will also be deposited onto the substrate with the assistance of the electric field and cause crack of the green films during the drying process.

(ii) *Deposition time*. In the initial stage, the thickness of the film increases almost linearly with the deposition time, which is in line with the equation proposed by Ishihara et al.[91] As the deposition proceeds further, the electric field started to drop with time and the deposition rate undergoes the same changes as well. The electric field became a function of the deposition time. Therefore, the deposition mass grow slowly and non-linearly, eventually reaching a maximum value at some point. The reason for the electric field decreases with the time is attributed to the shielding effects of the deposited insulating ceramic layer onto the substrates.

# *Chapter 4*

# Objectives

The microelectronics industry has constantly been seeking the solutions for the miniaturized, multifunctional and low-cost products. This in turn drives the search for the proper materials that meet the requirements.

As illustrated in the previous parts, tellurium based ceramics due to their low sintering temperatures might find application in microelectronics. The primary objective of this thesis, as stated by the title, is to investigate the fabrication and properties of copper tellurium based ceramics and thick films. In order to achieve this general goal, the following sub-objectives have to be accomplished in sequence:

1. Synthesis and characterization of $Cu_3TeO_6$ powders to be used as precursors for the fabrication of bulk ceramics and thick films. The conventional solid state reaction between copper oxide (CuO) and tellurium dioxide ($TeO_2$) will be used. The synthesis of monophasic precursor powders is a main aim and for that changes in the composition stoichiometry and in the calcination temperatures will be conducted. Compounds phase formation in the CuO-$TeO_2$ binary system will be studied as well.
2. Fabrication and characterization of $Cu_3TeO_6$ bulk ceramics. The sintering behavior of $Cu_3TeO_6$ ceramics will be studied in order to optimize the sintering conditions of the ceramics. Sintered ceramics will be characterized from the chemical, crystallographic, microstructural and dielectric response point of view.
3. Fabrication of thick films by electrophoretic deposition (EPD) and their characterization. Films will be deposited on both platinized silicon and copper foil. Silicon will be used as a proof of concept while copper

substrates target the applications in microelectronics to be embedded in circuitry and replace interfacial reaction layers. The relations between processing conditions and films properties will be established, by varying processing parameters as electric field, deposition time and sintering conditions.

4. Exploitation of sintering conditions of thick films on copper substrates. On one hand, copper is easily accessible and low-cost. On the other hand, it tends to be oxidized in oxidizing environment at high temperatures. Therefore, sintering $Cu_3TeO_6$ thick films on Cu foils is challenging. An alternative approach will be exploited.

# *Chapter 5*

## Experimental Procedures

In this chapter, the experimental techniques and procedures used in this work are presented. The major steps, as shown in Figure 14 and in accordance with the objectives defined for this work, are divided into four main sections: (1) synthesis and characterization of the precursors through solid state reactions of copper oxide (CuO) and tellurium dioxide ($TeO_2$); (2) sintering and characterization of the $Cu_3TeO_6$ bulk ceramics; (3) fabrication of $Cu_3TeO_6$ thick films by the electrophoretic deposition (EPD) method and their characterization; (4) attempts to sinter EDP $Cu_3TeO_6$ thick films on copper foil.

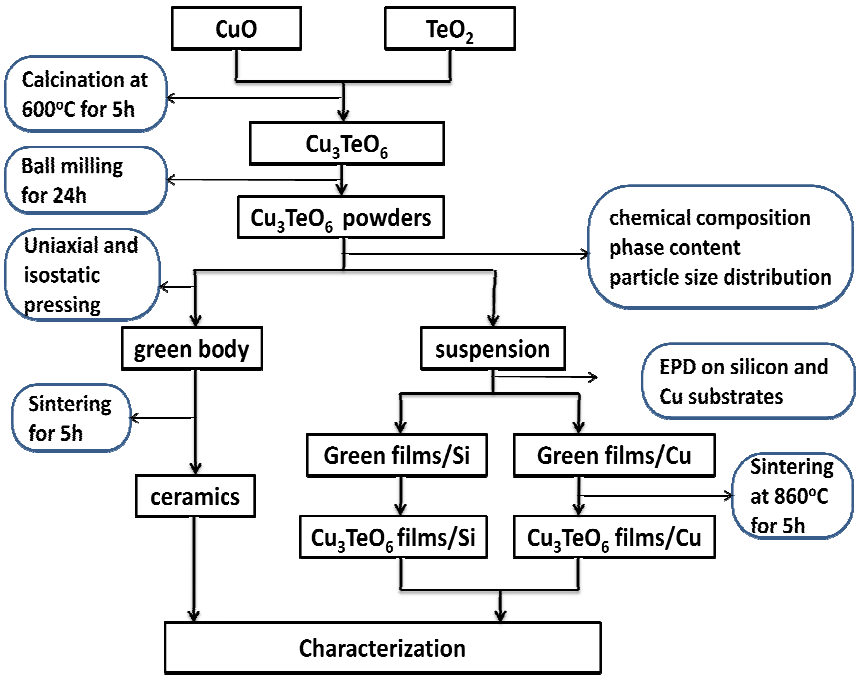


Figure 14. Flow chart of the experimental procedures

## 5.1 Chemical reagents

The starting materials used in the solid state reactions are reagent-grade copper oxide (CuO, The British Drug Houses LTD., purity>99%) and tellurium dioxide ($TeO_2$, Sigma-Aldrich, purity>99%). Before using them in the synthesis of the precursors, the reagents' chemical and purity were characterized. To prepare the suspensions for the electrophoretic deposition, acetone (Merck, >99.9%) was used as the solvent and triethanolamine (Merck, >99.9%) as the suspensions stabilizer.

## 5.2 Synthesis of $Cu_3TeO_6$ precursors

### 5.2.1 Ball milling

After weighing the oxides in the correct stoichiometries, the mixture was ball milled, aiming to form a homogeneous mixture of CuO and $TeO_2$ powders. In the meantime, the particle size of the powders can be reduced as well, leading to increased specific surface area and thus enhanced reactivity of particles during the solid state reactions.[92] In this work, a planetary ball mill was used to conduct the process. The raw powders were loaded together with ethanol into Teflon® containers. Yttrium-Stabilized-Zirconia (YSZ) balls with diameters of 5mm and 2mm in were used as the milling medium. The powders were ball milled for 24 hours at a constant speed of 200 rpm. After the ball milling, the mixture was dried at a temperature of 60$^{o}$C for 10 hours.

### 5.2.2 Calcination

The calcination was performed in an electric furnace chamber equipped with a Eurotherm® temperature controller (Model 2408). Copper oxide and tellurium dioxide powders with different molar ratios were calcined at temperatures ranging from 400$^{o}$C to 750$^{o}$C in air. The heating and cooling profile is shown as Figure 14.

5.2.3 Characterization of calcined powders

Thermogravimetric (TG) analysis and differential thermal analysis (DTA) of copper oxide and tellurium dioxide powders were conducted to study the phase transitions and kinetics of the solid state reactions. The heating rate was kept at $10^{o}$C/min.

To study the phase formation of the solid state reactions and the effects of temperatures and stoichiometry of starting materials, the powders obtained from calcinations under various conditions were characterized by X-ray diffraction (XRD, Rigaku, "Geigerflex" D/Max-B) analysis through *CuKα* radiation over the range of 2θ=10 to 90 degrees. Phase determination and calculation of the unit cell parameters were performed with Jade 6.0 (Materials Data, Inc.).

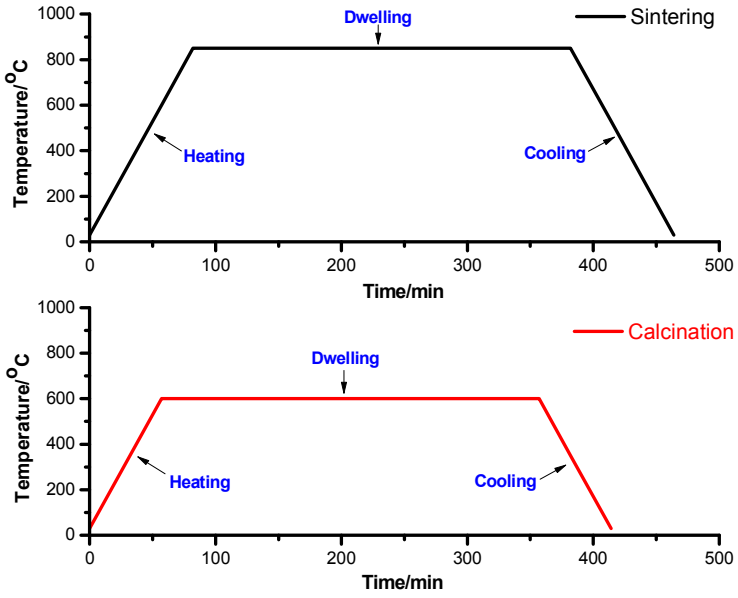


Figure 15. Heating and cooling profiles used in the calcination and sintering processes.

## 5.3 Fabrication of $Cu_3TeO_6$ ceramics

The calcined $Cu_3TeO_6$ powders were used to fabricate bulk ceramics. Ball milling was applied to reduce the particle size of the $Cu_3TeO_6$ powders.

Subsequently, the dried powders were pressed into disks in two steps: uniaxial pressing at 25 MPa and an isostatic pressing under a pressure of 200MPa for 5 minutes. For each sample, around 0.5g of powders was used and the disks are roughly 10mm in diameter and 4mm in thickness. No binder was added during the pressing process.

Sintering of the green bodies was performed at different temperatures (750$^{o}$C-900$^{o}$C) in an electric radiant tubular furnace equipped with a Eurotherm® temperature controller. The sintering temperature programming is similar to that of the calcination step, as shown in Figure 15: both heating and cooling rates are 10$^{o}$C/min and dwelling time is 300min. Due to the high volatility of tellurium dioxide,[93] the samples were held in a closed alumina crucible to reduce the evaporation of $TeO_2$.

## 5.4 Fabrication of $Cu_3TeO_6$ thick films

5.4.1 Electrophoretic deposition (EPD)

The EPD process began with the preparation of the suspensions. As previously described, a stabilized suspension with well-dispersed particles is critical to the deposition. Based on the work by Su et al.,[37] acetone and triethanolamine are used as the liquid medium and the stabilizer, respectively.

The accurately weighed $Cu_3TeO_6$ powders (0.5g) were dispersed into the solvent (100ml) with the assistance of a sonicator. And then, the suspension was switched to a constant magnetically stirring for 4h. 2ml of triethanolamine (TEA) were added to achieve high surface charge of the particles.

In this work, a home-made EPD set-up was used to carry out the $Cu_3TeO_6$ thick films deposition. The basic functional components of the device include a DC voltage supplier, a beaker for containing the suspension, two Teflon® cells for fixing the substrates and counter electrode, a Teflon® base for the installation of the cells.

To study the deposition kinetics, different voltages and deposition time were applied. The external electric field was provided by a DC power supplier (EPS HV 5006-400, Glassman High Voltage INC.). DC voltages varying from 50V to 400 V were applied to the substrate on the negative pole with respect to the counter electrode. The deposition time varies from 1 minute to 6 minutes under a constant applied voltage. In this work, the platinized silicon (Inostek Inc.) and copper foil (thickness 25 μm) were employed as the substrate materials while the platinum was used as counter electrode. It is worth noting that a sonication process and magnetic stirring are conducted before each deposition operation. The readily prepared films were dried at room temperature for at least 24 hours before further characterizations and sintering.

5.4.2 Sintering of the thick films

The green-body films were sintered in the same tubular electric furnace as the one used for the sintering of $Cu_3TeO_6$ bulk ceramics. Due to the high aspect ratio of the films, the volatilization of tellurium component may be favored at high temperatures. In order to control this volatilization, a small amount of $TeO_2$ powders were placed inside the closed alumina crucible to create a high partial pressure of tellurium and thus suppress the tendency for tellurium evaporation during the sintering process. The green films were sintered at temperatures ranging from 800$^{o}$C to 860$^{o}$C.

## 5.5 Characterization of $Cu_3TeO_6$ ceramics and thick films

For the bulk $Cu_3TeO_6$ ceramics, the dimensions and weights of both the green and sintered pellets were precisely measured to calculate weight loss, volumetric shrinkage, geometrical density and relative density. A Vernier caliber and a micrometer were used for the dimension measurements of the ceramic and thick films, respectively.

X-ray diffraction (XRD) analysis was conducted to investigate the phase formation process and phase stability of $Cu_3TeO_6$ ceramics and thick films after

being sintered under different conditions. To avoid any preferential crystallographic orientation, $Cu_3TeO_6$ ceramics were ground into fine powders before XRD and placed in a zero-background sample holder.

For microstructural analysis $Cu_3TeO_6$ ceramics and films were observed by scanning electron microscopy (SEM) with a Hitachi S-4100 SEM.

To perform the electrical measurement, gold electrodes with diameter of 9mm and 0.6 mm for the thick films) were deposited through a shadow mask on the surfaces of the ceramics and thick films, respectively. In the case of the ceramics the electrodes were deposited on both sides of the sintered $Cu_3TeO_6$ disks to form MIM (metal/insulator/metal) capacitors. After the deposition, the ceramic disks and thick films were annealed at $80^oC$ for 20 min to improve the interface of gold / ceramic. Dielectric permittivity, loss tangent and the temperature coefficient of permittivity of $Cu_3TeO_6$ ceramics were measured with a precision LCR meter (4284A, Hewllet Packard) over a frequency ranging from 1 KHz to 1MHz at different temperatures.

# Chapter 6

# Results and Discussion

In this chapter, the obtained results will be presented and analyzed.

## 6.1 Precursor synthesis

The precursors for this work were synthesized by the conventional solid state reactions between copper oxide and tellurium dioxide powders. Depending on the molar ratios of the starting materials and heating temperatures, the products with different chemical compositions were yielded from the calcination processes performed in air. In this work, three different compositions: $CuO+TeO_2$, $CuO+2TeO_2$ and $3CuO+TeO_2$, were prepared and the phase formation of the within $CuO-TeO_2$ binary system was studied.

Figure 16 depicts the XRD patterns of the products of the aforementioned three compositions calcined at $600^oC$. $Cu_3TeO_6$ and $CuTe_2O_5$ are obtained as the monophasic products of the $3CuO+TeO_2$ and $CuO+2TeO_2$ compositions, respectively. The calcination of the $CuO+TeO_2$ composition gave rise to a mixture of $Cu_3TeO_6$ and $CuTe_2O_5$.

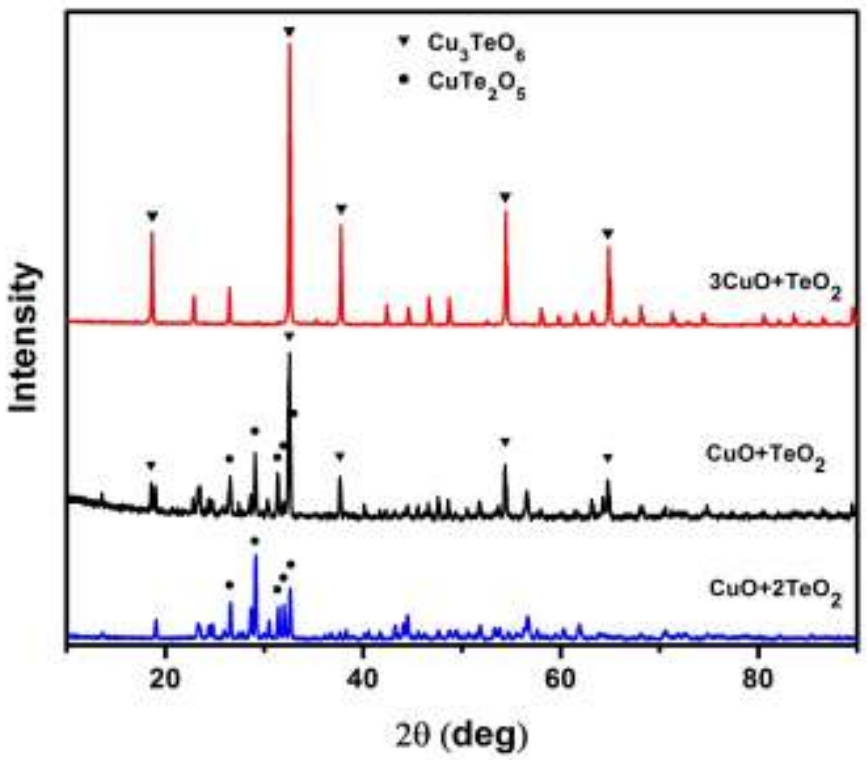


Figure 16. X-ray diffraction patterns of $CuO+TeO_2$, $CuO+2TeO_2$ and $3CuO+TeO_2$, calcined at 600°C. Monophasic $Cu_3TeO_6$ and $CuTe_2O_5$ powders were obtained for $3CuO+TeO_2$ and $CuO+2TeO_2$, respectively.

6.1.1 The $3CuO+TeO_2$ system

The powders of the $3CuO+TeO_2$ composition were calcined at the temperatures ranging from 550°C to 700°C and $Cu_3TeO_6$ was determined to be the only compound from the X-ray diffraction patterns of the products, as shown in Figure 17. In the solid state reaction, the tetravalent tellurium ($Te^{4+}$) was oxidized to hexavalent tellurium ($Te^{6+}$). Without taking into consideration of the intermediate products yielded during the heating process, the formula of the overall reaction involving the oxidation is shown as below:

$$3CuO + TeO_2 + \frac{1}{2}O_2 \rightarrow Cu_3TeO_6$$

The crystal structure of $Cu_3TeO_6$ synthesized in this work was determined by Jade® to be cubic, *Ia3* and the unit cell parameter a=9.538Å. The data matches the results reported by Hostachy *et al.* very well.[55]

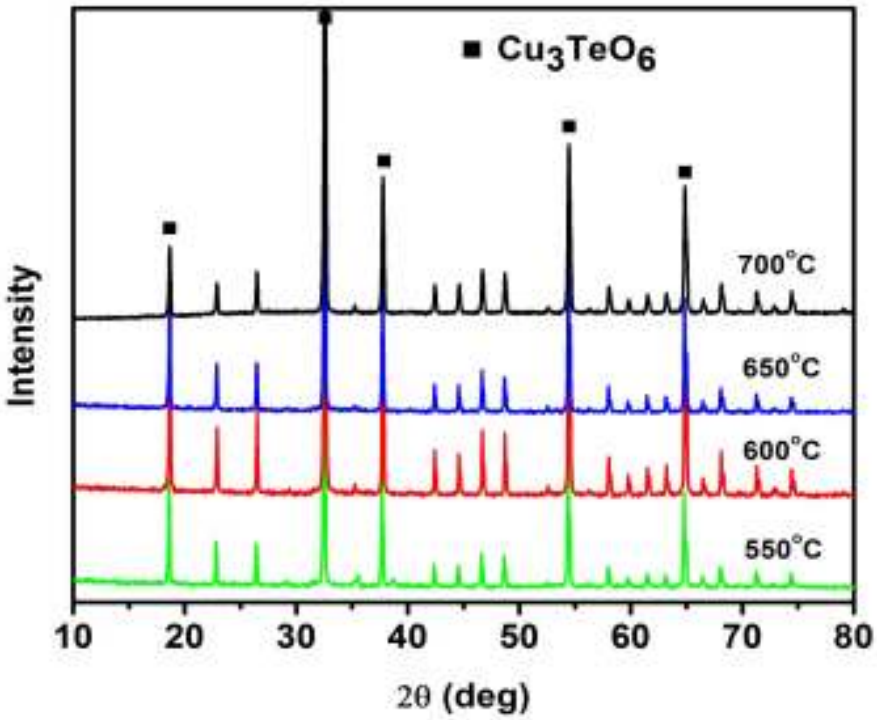


Figure 17. X-ray diffraction patterns of the $3CuO+TeO_2$ composition calcined at different temperatures. The formed phase is $Cu_3TeO_6$.

Thermogravimetric analysis (TG) and differential thermal analysis (DTA) data of the $3CuO+TeO_2$ mixture are shown in Figure 18. At temperatures lower than 450°C, no obvious weight change is indicated in the thermogrametric profile. Therefore, the oxidation reaction did not take place in this temperature range. As the temperature was raised to about 450°C, a weight gain at a relatively low rate occurred. This gain is attributed to an oxidation reaction, during which the tetravalent tellurium ($Te^{4+}$) was oxidized into hexavalent tellurium ($Te^{6+}$), resulting in the formation of the $Cu_3TeO_6$ phase. With further increase of the temperature up to 550°C, the weight gain increased at a much higher rate, suggesting a faster oxidation reaction. The rapid change of reaction rate could be

caused by the formation of a eutectic of $Cu_3TeO_6$ and the intermediate product $CuTeO_3$, which was proposed by Ivanova *at al.*[61] in the phase diagram of the $CuO$-$TeO_2$ system. The diffusion of the solid particles was greatly promoted by the eutectic liquid and hence the reaction rate was enhanced. The theoretical weight gain due to the oxidation reaction is calculated to be 3.86%, according to the proposed reaction formul. Experimental value of the weight gain is 3.83%, as shown by the thermogravimetric analysis data. The calculated and measured values agree quite well, supporting the suggested oxidation and reaction mechanism formation.

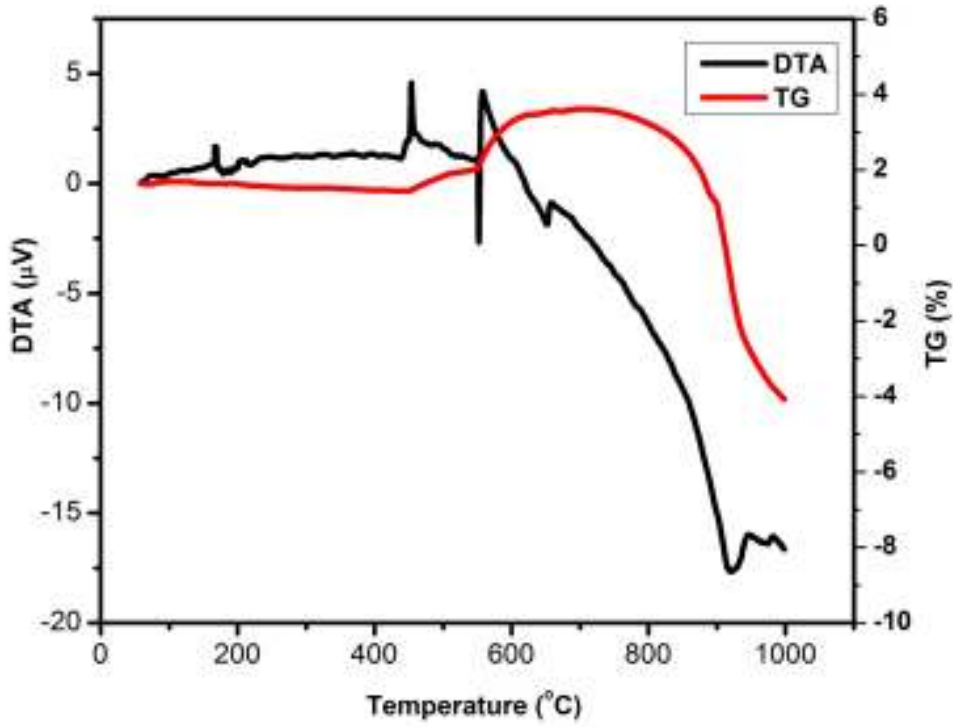


Figure 18. Thermogravimetric and differential thermal analysis data of the composition $3CuO+TeO_2$

At around 730°C, the weight started to decrease and this might result from the volatilization of tellurium dioxide which has a melting point of 733°C. The

rapid decomposition of $Cu_3TeO_6$ took place after 870°C, causing a rapid weight loss in the system.

### 6.1.2 The $CuO+TeO_2$ system

The powders of $CuO+TeO_2$ (1:1) were calcined at 400°C, 500°C and 600°C. No monophasic product was obtained from the solid state reactions at any of these temperatures. According to the XRD data (Figure 19), three compounds: $CuTe_2O_5$, $Cu_3TeO_6$ and $CuTeO_3$, were formed at 400°C and 500°C while $CuTe_2O_5$ and $Cu_3TeO_6$ were detected at 600°C.

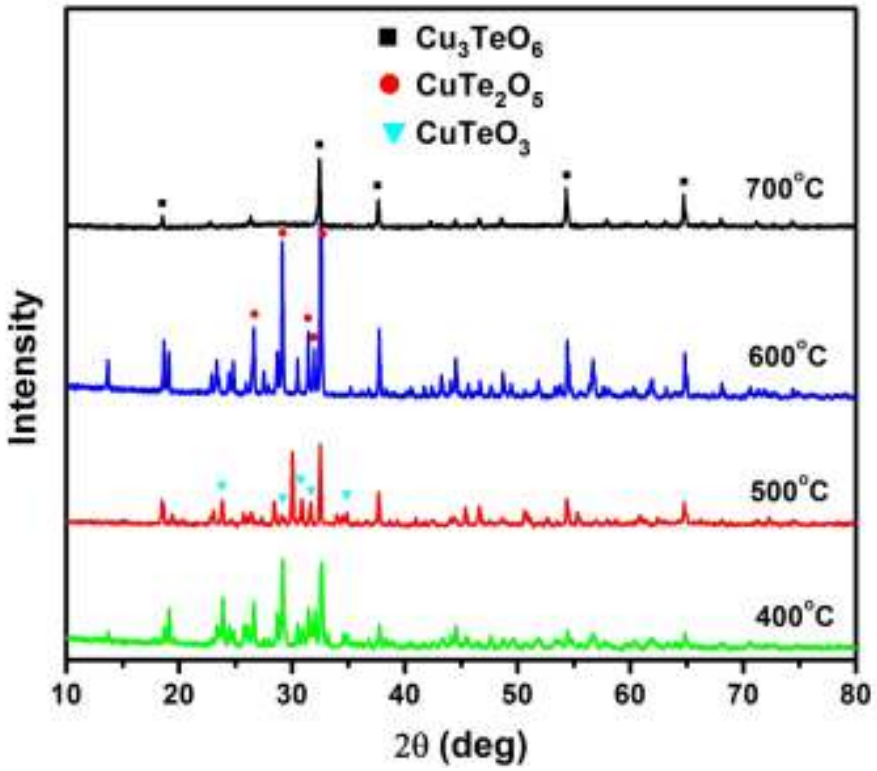


Figure 19 X-ray diffraction patterns of the composition $CuO+TeO_2$ calcined at 400°C, 500°C and 600°C. No monophasic composition was obtained in this system.

From the XRD data it was observed that at low temperatures, below 400°C for instance, the solid state reaction between copper oxide and tellurium dioxide took place, forming a mixture of $CuTeO_3$, $CuTe_2O_5$ and $Cu_3TeO_6$.

As the calcination temperature increased (400°C to 500°C) $CuTeO_3$ was oxidized and two compounds, $CuTe_2O_5$ and $Cu_3TeO_6$ were formed. At this temperature three compounds co-exist in the product.

$$CuTeO_3 + \frac{1}{2}O_2 \rightarrow Cu_3TeO_6 + 2CuTe_2O_5$$

With further increase of the temperature, for instance to 600°C, the $CuTeO_3$ phase will be completely reacted, giving rise to the binary products of $CuTe_2O_5$ and $Cu_3TeO_6$.

## 6.2 Particle size analysis

The particle size and its distribution play an important role in the sintering behavior of bulk ceramics. Moreover, the quality of the films fabricated by the electrophoretic deposition (EPD) method is affected by the particle size and particle size distribution, as well. Small particles due to their enhanced reactivity facilitate the densification process. On the other hand small particles form homogeneous and stable suspensions that originate homogeneous and crack-free thick films.

Therefore, the synthesized monophasic $Cu_3TeO_6$ powders were subject to the ball milling process to reduce the particle size before use in the ceramics and thick films fabrication.

The particles size analysis results of the milled powders are shown in Figure 20. There is a bimodal distribution of the particle size, with over 90% of the particles smaller than 3.6 μm while the average particle size is around 1.3 μm. The results

are in accordance with what was observed in the SEM images of the as-deposited films (Figure 37).

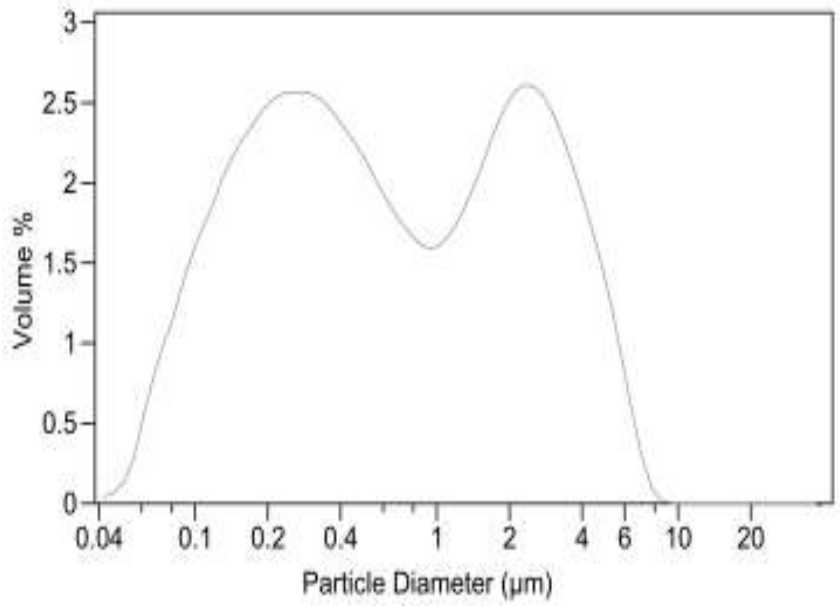


Figure 20. Particle size distribution of $Cu_3TeO_6$ powders after ball milling for 48h

### 6.3 Sintering of $Cu_3TeO_6$ ceramics

Conventionally, the sintering behaviors of ceramics reflected in densification can be determined by the dilatometric analysis, where the shrinkage of the green body is measured as a function of the temperature during the heating process. However, the lack of data on the melting point of $Cu_3TeO_6$ and the high volatility of copper oxide and tellurium dioxide raised the risk of equipment contamination, making the dilatometry method no longer feasible in this work, under the current experimental facilities of the Department of Ceramics and Glass Engineering. Alternatively, the sintering behavior and the shrinkage and relative density profiles of $Cu_3TeO_6$ ceramics were obtained by plotting the volume shrinkage and relative densities of the ceramics versus sintering temperatures determined for different sintering temperatures (Figure 21).

The disks of $Cu_3TeO_6$ green body were sintered at a series of temperatures ranging from 750°C to 900°C. At the temperatures of 870°C and above, the warpage of the sintered ceramic was so significant that it is no longer possible to accurately determine the volume shrinkage. Therefore, the profile only shows the data obtained up to the 865°C.

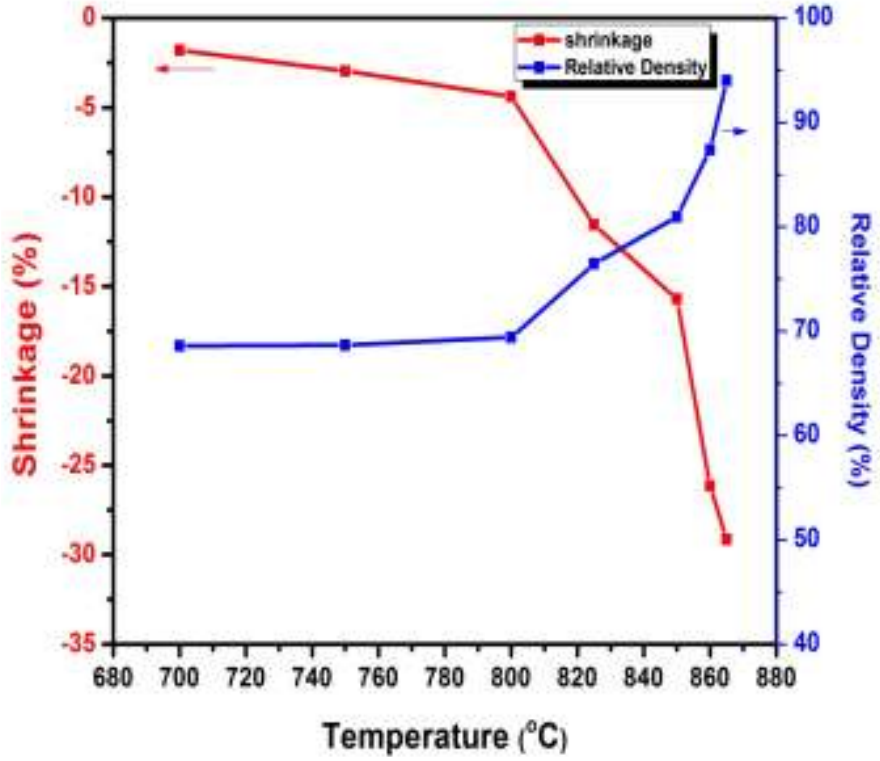


Figure 21. The variation of volumetric shrinkage and relative density of $Cu_3TeO_6$ ceramic with the sintering temperatures

Densification of the $Cu_3TeO_6$ ceramics started temperature between 800 and 820°C. For temperatures higher than 850°C, the shrinkage and the relative density change rapidly. The relative density of the ceramic reaches 89% and 93% when sintered at 860°C and 865°C, respectively. Compared with other tellurium-based compositions, such as $TiTe_3O_8$ (720°C)[42] and $Ba_2Te_2O_8$ (650°C),[94] $Cu_3TeO_6$ has a higher sintering temperature yet lower than that of $Ba_2TeO_5$ (950°C).

Figure 22 is a photograph of a sintered ceramic disk on top of the platinum substrate used as the sample holder (the alumina cover is shown as well) after being sintered at 900°C. The volatilization of copper oxide and/or tellurium dioxide must have taken place during the sintering process and a diffusion within the sample holder is clearly seen. Besides the sample is melted.

In order to study the compositional change, the sintered ceramic were characterized by XRD analysis (Figure 23).

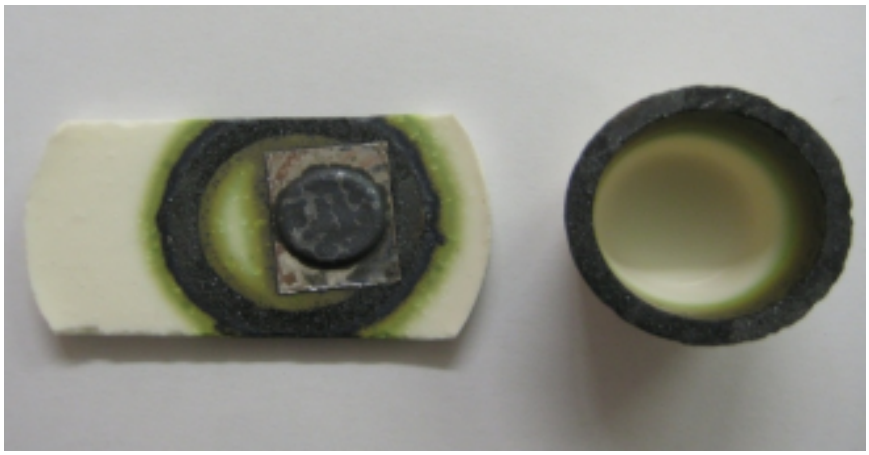

Figure 22. $Cu_3TeO_6$ ceramic, sample holder and cover after being sintered at 900°C. The diffusion of Cu and Te is obvious.

Comparing with the monophasic green body, the XRD pattern indicates that copper oxide (CuO) and $Cu_3TeO_6$ phases co-exist in the ceramic sintered at 900°C. At these temperatures $Cu_3TeO_6$ has been partially decomposed; the highly volatile tellurium dioxide was vaporized during the sintering process originating the appearance of copper oxide together with $Cu_3TeO_6$.

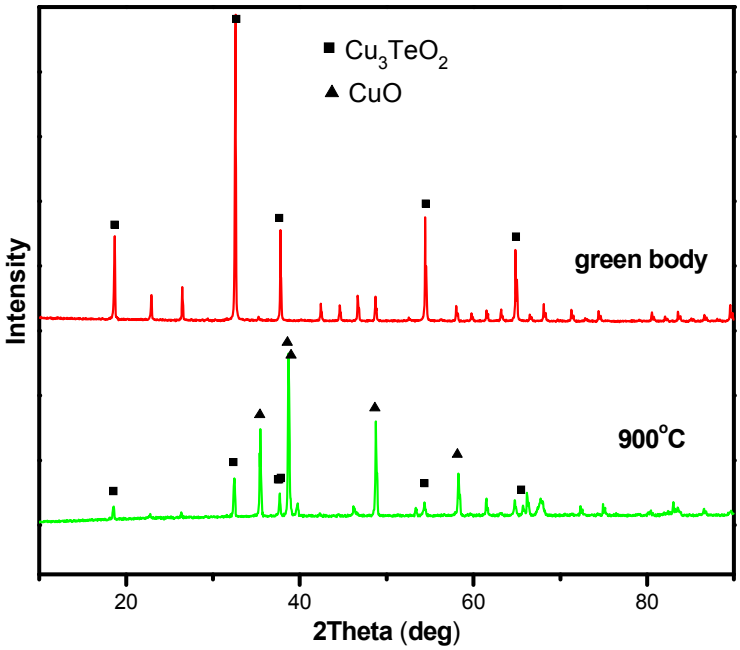


Figure 23. XRD patterns of the $Cu_3TeO_6$ green body and the ceramics after the sintering at 900°C. The decomposition of $Cu_3TeO_6$ occurs with the formation of CuO after sintering at 900°C.

## 6.4 Characterization of $Cu_3TeO_6$ ceramics

### 6.4.1 X-ray diffraction analysis

Tellurium (Te) is known to have low vapor pressure so it is likely to vaporize at high temperatures, especially when the partial pressure of Te in the atmosphere is low with respect to that in the bulk ceramic. The $Cu_3TeO_6$ ceramics sintered at various temperatures were characterized by XRD analysis analysis to study compositional stability and the XRD patterns are shown in Figure 24.

As suggested by the comparison of XRD patterns, the composition of $Cu_3TeO_6$ ceramics sintered at 860°C and 865°C is identical to that of the green body. $Cu_3TeO_6$ is stable at and below 865°C.

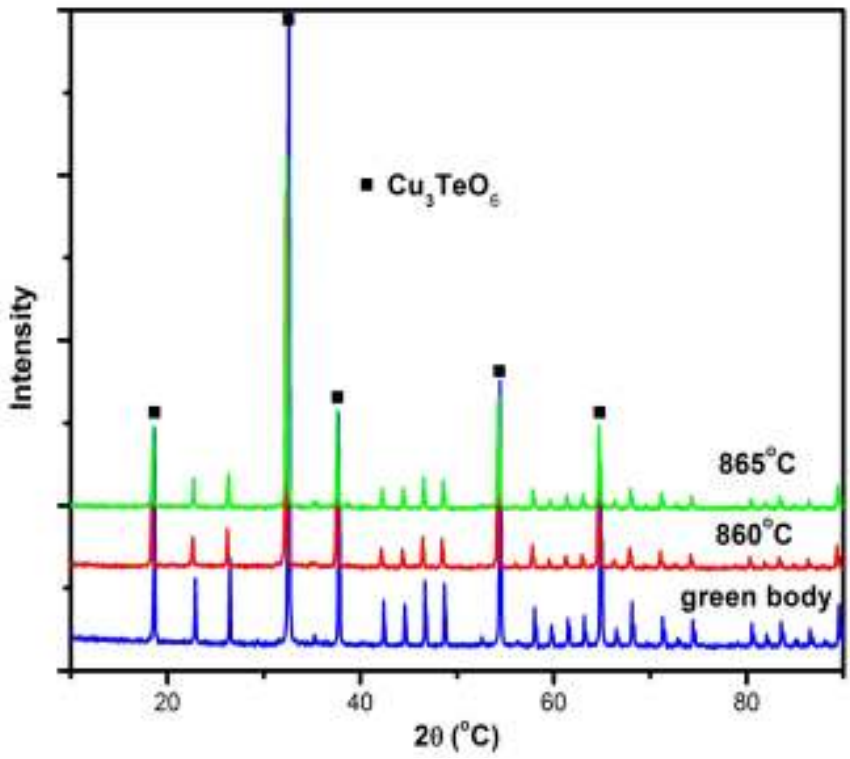


Figure 24. XRD patterns of $Cu_3TeO_6$ green body and ceramics sintered at 860°C and 865°C. No decomposition of the $Cu_3TeO_6$ phase is observed at these sintering temperatures.

6.4.2 Microstructural analysis

The microstructure of the $Cu_3TeO_6$ ceramics sintered at different temperatures was assessed by SEM. The micrographs of the fracture surface of the ceramics are shown in Figures 25 to Figure 27.

For the sample sintered at 750°C (Figure 25), no significant grain growth was observed and the particles are still discretely distributed. Most of the particles have a diameter of less than 3.5 µm. The larger particles remain the plate-like

shape. The volumetric shrinkage and relative density are 2.96% and 68.67%, respectively.

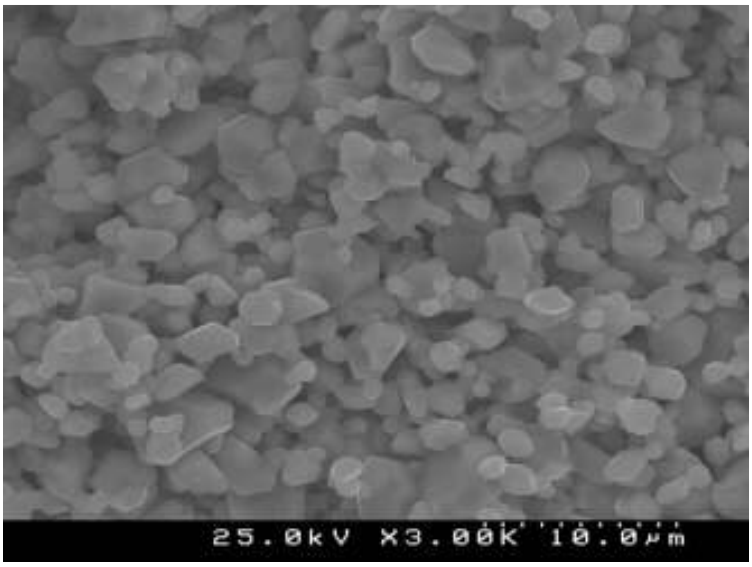


Figure 25. Fracture surface micrograph of $Cu_3TeO_6$ ceramics sintered at 750$^{o}$C

After sintering at 860$^{o}$C, a densified ceramic was obtained. The grain growth was greatly promoted (Figure 26), though the grain size distribution is not uniform. Compared with the previous microstructures the grains have mainly a dodecahedron shape, characteristic of a final stage of densification. A relative density higher than 89% was achieved. The SEM micrograph of the ceramic sintered at 865$^{o}$C (Figure 27) indicates the existence of a liquid phase during the sintering process. The resultant ceramic has a relative density of 93% and a volumetric shrinkage of 29%.

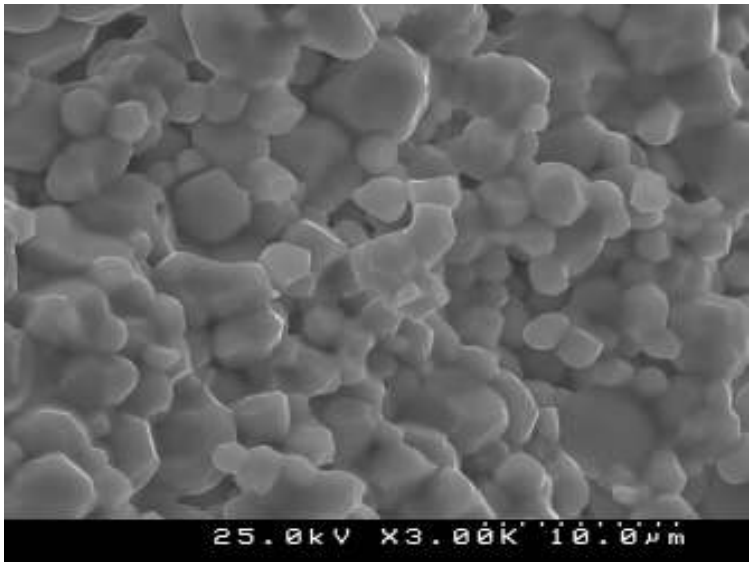


Figure 26. Fracture surface micrograph of $Cu_3TeO_6$ ceramics sintered at 860$^oC$

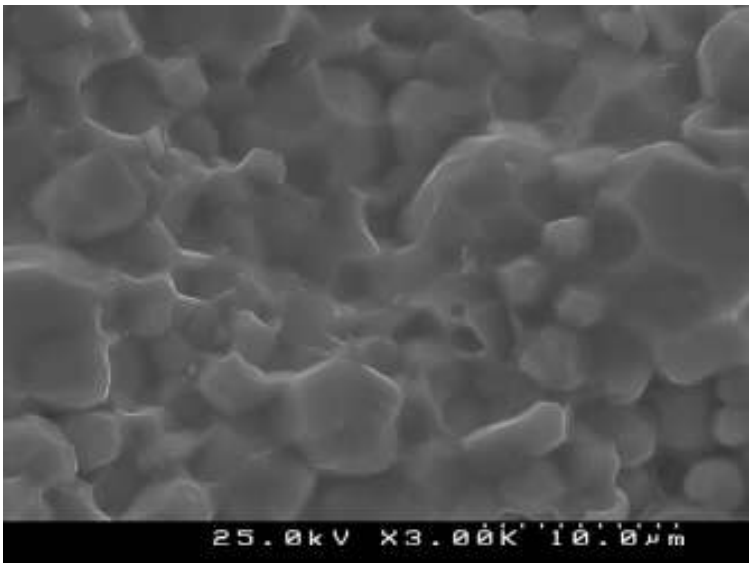


Figure 27. Fracture surface micrographs of $Cu_3TeO_6$ ceramics sintered at 865$^oC$

6.4.3 Electrical measurements

The relative permittivity ($\varepsilon_r$) of the $Cu_3TeO_6$ ceramics sintered at 865$^oC$ (Figure 28) varies between 38.3 and 12.7 within the frequency range of 1 KHz and 1 MHz. It shows a strong dependence on the frequency of the measurement

at room temperature. With the increase of the frequency, $\varepsilon_r$ value falls rapidly, following a typical dielectric relaxation process.

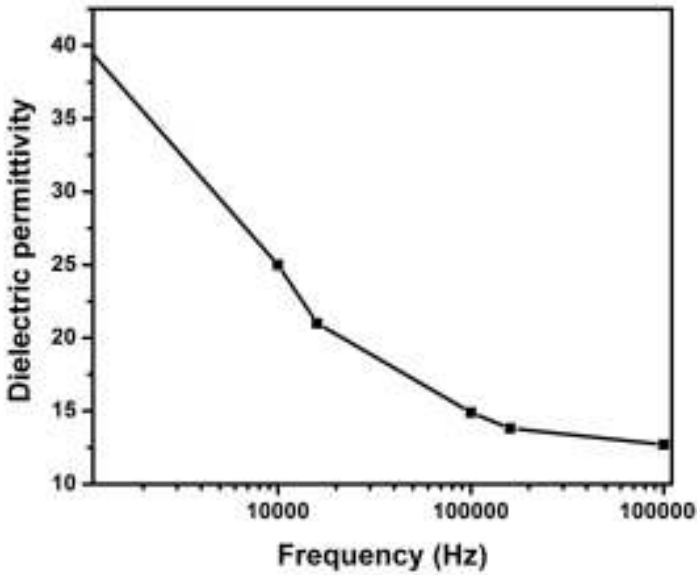


Figure 28. Relative permittivity at room temperature for the $Cu_3TeO_6$ ceramics sintered at 865$^oC$

The loss tangent of the $Cu_3TeO_6$ ceramics sintered at 865$^oC$ increases with the frequency of measurement to a maximum value 0.42 at around 100 KHz and then decreases to 0.1 at 1 MHz (Figure 29). In this range, the frequency has a dual impact on the loss tangent.

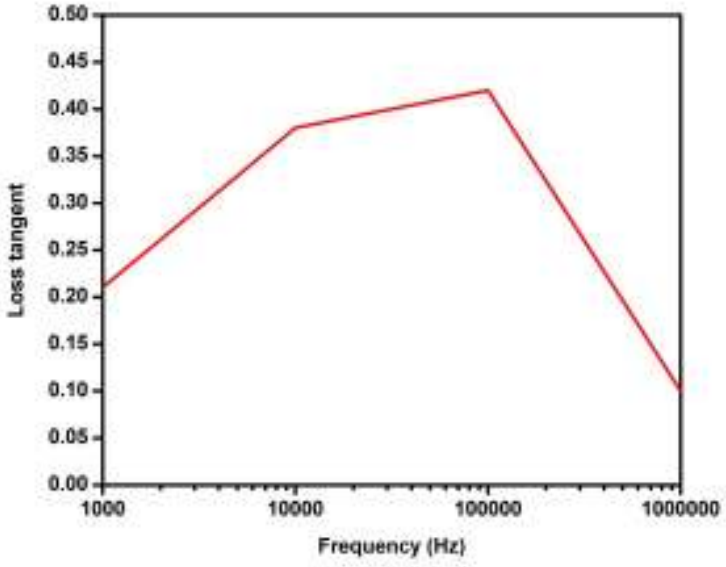


Figure 29 Loss tangent for at room temperature for the $Cu_3TeO_6$ ceramics sintered at 865$^oC$

The dielectric permittivity as a function of the temperature measured at different frequencies for $Cu_3TeO_6$ ceramics sintered at various temperatures is plotted in Figures 30 to 34. For all the ceramics, the dielectric permittivity doesn't vary significantly with the temperature; this temperature stable variation is more obvious for the samples sintered at low temperatures what is is related to the their low density. The ceramics sintered at 865$^oC$ have a much higher dielectric permittivity than those sintered at lower temperatures. The behavior clearly reflects the densification of the ceramics sintered at high temperatures. And the permittivity difference decreases with the frequency.

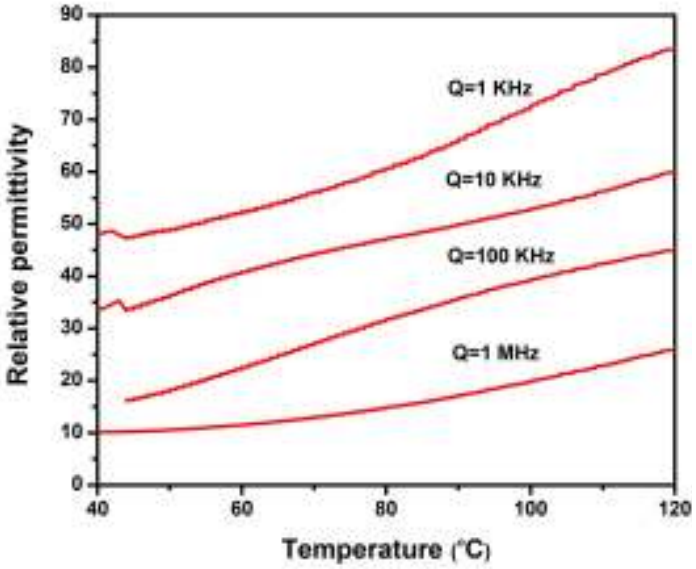


Figure 30. Temperature dependence of dielectric permittivity of $Cu_3TeO_6$ ceramics sintered at 865°C.

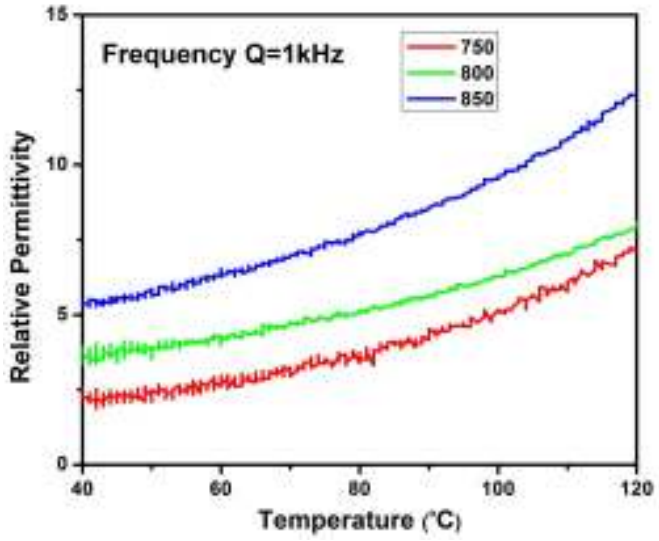


Figure 31. Temperature dependence of dielectric permittivity of $Cu_3TeO_6$ ceramics sintered at different temperatures (measured at the frequency of 1 KHz)

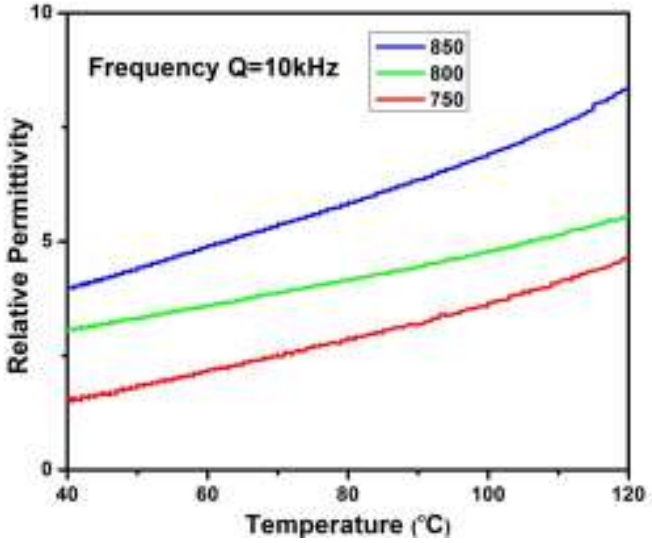


Figure 32. Variation of dielectric permittivity of $Cu_3TeO_6$ ceramics sintered at different temperatures (measured at the frequency of 10 KHz)

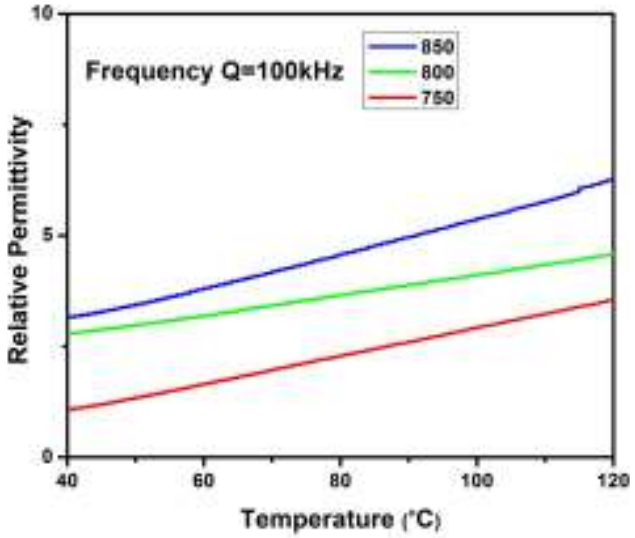


Figure 33. Variation of the dielectric permittivity of $Cu_3TeO_6$ ceramics sintered at different temperatures (measured at the frequency of 100 KHz)

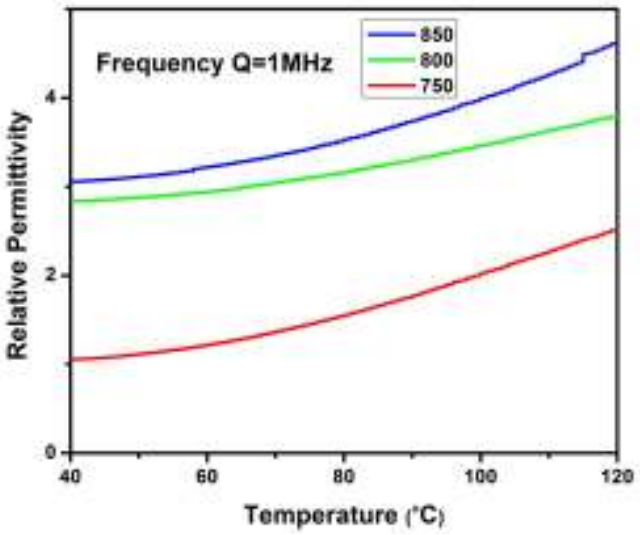


Figure 34. Variation of the dielectric permittivity of $Cu_3TeO_6$ ceramics sintered at different temperatures (measured at the frequency of 1 MHz)

The temperature coefficient of the dielectric permittivity ($TC\varepsilon_r$) is calculated by the equation:

$$TC\varepsilon_r = \frac{\Delta\varepsilon_r}{\Delta T}\frac{1}{\varepsilon_o}$$

where $\Delta\varepsilon_r$ stands for the change in relative dielectric permittivity within the temperature change, from 40°C to 120°C in this work, and $\varepsilon_o$ for the permittivity at 40°C. The temperature coefficient of dielectric permittivity for differently sintered ceramics is shown in Table 3.

Table 3 Temperature coefficient of the dielectric permittivity ($TC\varepsilon_r$/ppm·$^oC^{-1}$ ·$10^4$) of $Cu_3TeO_6$ sintered at different temperatures

| Sintering temperature | Frequency | | |
|---|---|---|---|
| | 10 KHZ | 100KHz | 1 MHz |
| 750$^o$C | 2.52 | 2.86 | 1.72 |
| 800$^o$C | 1.02 | 0.81 | 0.43 |
| 850$^o$C | 1.38 | 1.23 | 0.64 |
| 865$^o$C | 1.05 | 2.36 | 2.04 |

The temperature coefficient of dielectric permittivity of the $Cu_3TeO_6$ ceramics exhibits very high positive values, ranging from $0.43\times10^4$ ppm·$^oC^{-1}$ to $2.36\times10^4$ ppm·$^oC^{-1}$. According to the requirements of LTCC materials: controlled dielectric permittivity, low loss and near-zero temperature coefficient of the dielectric permittivity are needed. From the point of the application of $Cu_3TeO_6$ ceramics in the LTCC technology will require some optimization. The improvement in $TC\varepsilon_r$ might be obtained by the formation of multiphasic systems with the compositions that have high negative $TC\varepsilon_r$ values.

## 6.5 Fabrication of $Cu_3TeO_6$ thick films

### 6.5.1 Deposition and deposition conditions: influence of applied voltage and deposition time

Under the current experimental conditions and using a suspension of $Cu_3TeO_6$ powders in acetone stabilized with triethanolamine, it was observed that green films of $Cu_3TeO_6$ were formed on the substrate connected to the cathodic electrode of the DC power supplier. Therefore, the electrophoretic deposition in this work should be classified as the “cathodic EPD”, which in turn indicates that the particles in the suspension acquired positive surface charges.

As described Chapter 3, for a specific suspension system and EPD device, the applied voltage and deposition time have significant impact on the deposition process and on the final thickness and film quality. Figure 35 and 36 depict the thickness of deposited $Cu_3TeO_6$ green films as a function of the deposition time and applied voltage, respectively.

Under the electric field of 100V, the film thickness grew to around 24 μm in 1 minute and 47 μm in 2 minutes, showing a linear dependence on the time. However, the deposition rate dropped dramatically in the later stage, due to the shielding effect of the deposited film acting as an insulating layer. At 200V, the deposition rate at the first one minute is very high and reached a plateau after the first minute. The thickness increased only 5 μm when the deposition was prolonged to 4 minutes.

With the increased deposition time, the films become less uniform in terms of the surface roughness. The upper part of the film on the substrate, which is vertically placed in the suspension, is thinner and less rough than the lower part, where some bumps are distributed. The reason is attributed to the fact that large particles tend to settle due to the gravity and thus a gradient is formed in the suspension. If the electrophoretic mobility of the larger particles is not able to suppress the gravitational mobility, finer particles will be deposited on the upper part while the coarser ones are deposited on the lower part.

When changing the electric field for a fixed deposition time, the film thickness increased almost linearly with the voltage, as shown in Figure 35. Strong electric fields, above 300V in this work, grant that the coarse particles electrophoretic mobility will be high enough to overcome their gravity and thus deposited, resulting in the deterioration of the film quality.

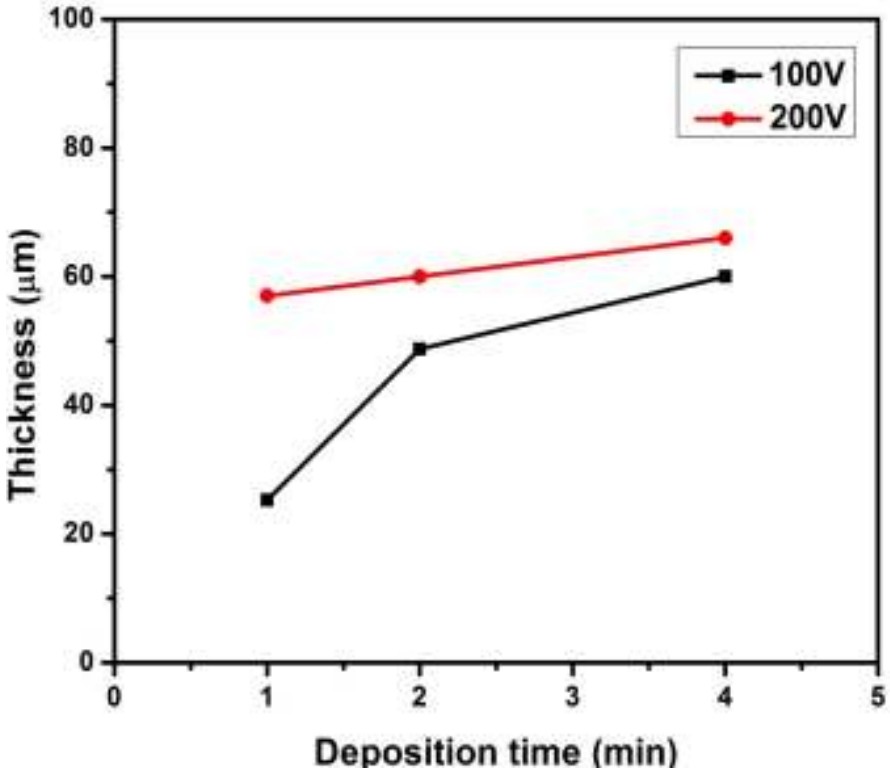


Figure 35. The thickness of $Cu_3TeO_6$ green films plotted as a function of the deposition time, for two different applied voltages

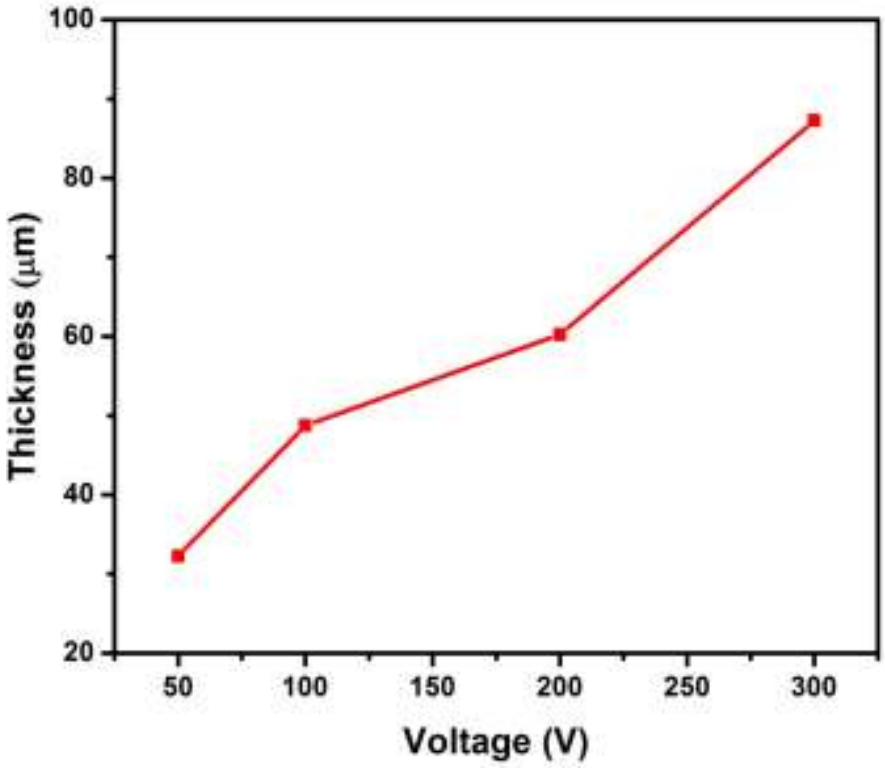


Figure 36 The thickness of $Cu_3TeO_6$ green films as a function of the applied voltages, for deposition time of 2min

6.5.2 X-ray diffraction analysis

Due to their large aspect ratios, the chemical composition of the thick films is more liable to be altered during the sintering process, compared with that of the bulk ceramics. Therefore, attention should always be paid to the phase stability of the thick films after the sintering process. Figure 37 shows the XRD patterns of $Cu_3TeO_6$ thick films sintered at temperatures ranging from 800$^{o}$C to 860$^{o}$C. No immediate change in chemical composition and crystal structure is detected and $Cu_3TeO_6$ remained the only phase.

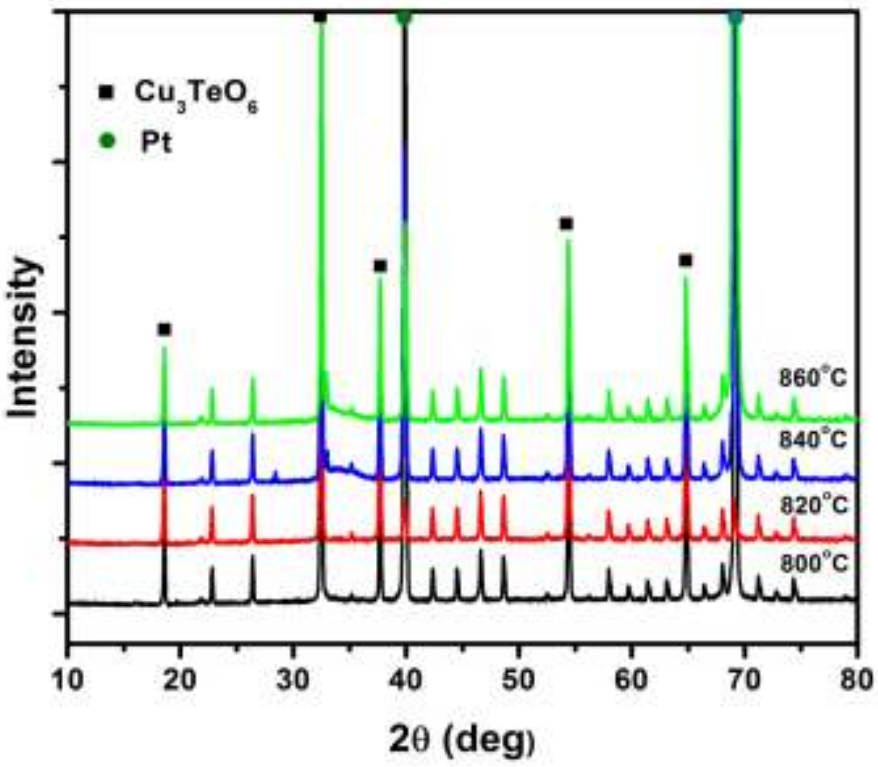


Figure 37. X-ray diffraction patterns of $Cu_3TeO_6$ thick films sintered at different temperatures

## 6.6 Characterization of $Cu_3TeO_6$ thick films

### 6.6.1 Microstructural properties of the as-deposited and sintered films

Figure 38 illustrates the surface optical image of a dried film $Cu_3TeO_6$ film deposited at 100 V during 2 min in which the surface is very homogeneous and no cracks are observed.

As shown by the SEM micrographs of the surface of the as-deposited films (Figure 39), the particles are loosely packed and most of them have diameters lower than 2 µm, indicating that the coarse particles settled in the suspension during the deposition process.

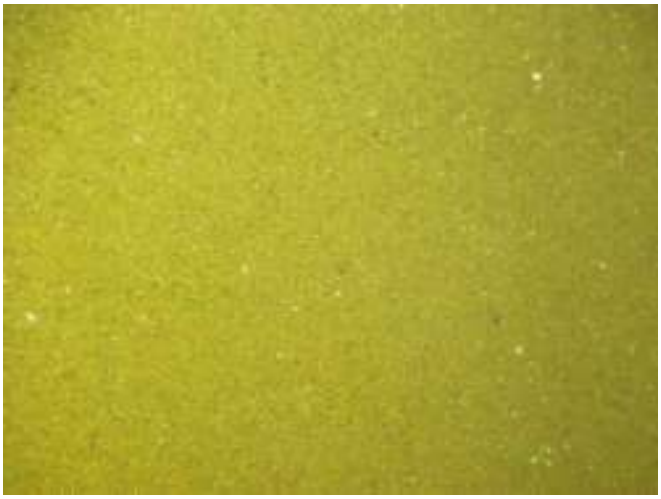

Figure 38. Surface image of Cu3TeO6 green films by optical microscopy (10x). The film was at 100 V and during 2 min.

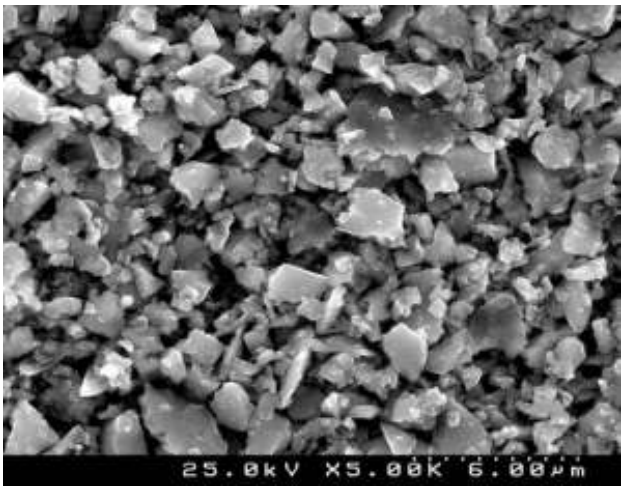


Figure 39. SEM surface micrograph of $Cu_3TeO_6$ green films deposited under 100 V and during 2 min.

The films sintered at 820$^{o}$C for 5 hours exhibit a densified microstructure with obvious grain necks and grain boundaries (Figure 40). Most of the grains have diameters in the range of 1 µm to 2 µm and the grain growth is not significant. In addition, some porosity is clearly seen.

Figure 41 depicts the cross-section SEM micrograph of a thick film sintered at 860$^{o}$C. The thickness of the sintered film is around 50. This value is slightly smaller than that of the green film which is 52 µm, indicating shrinkage of 4% in the direction of normal to the film. The microstructure of the film is quite homogenous and there are no appreciable thickness differences along the films. The micrograph reveals some porosity although homogeneously distributed, corroborating the top view micrograph. The surface roughness is also low. From the top-view SEM image (Figure 42), the densification of this film sintered at a higher temperature improved and the grains grew significantly when compared with equivalent films sintered at lower temperatures. A large portion of the grains have diameters of larger than 4 µm.

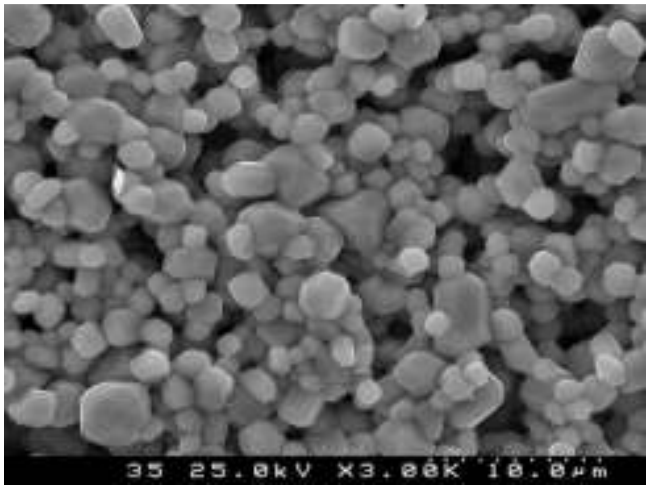


Figure 40. SEM micrograph of the surface image of $Cu_3TeO_6$ film sintered at 820$^{o}$C by SEM.

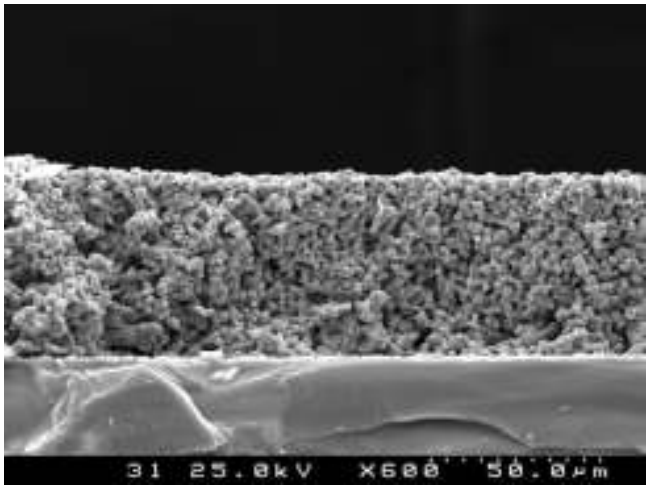


Figure 41. SEM cross-section micrograph of $Cu_3TeO_6$ film sintered at 860$^{o}$C.

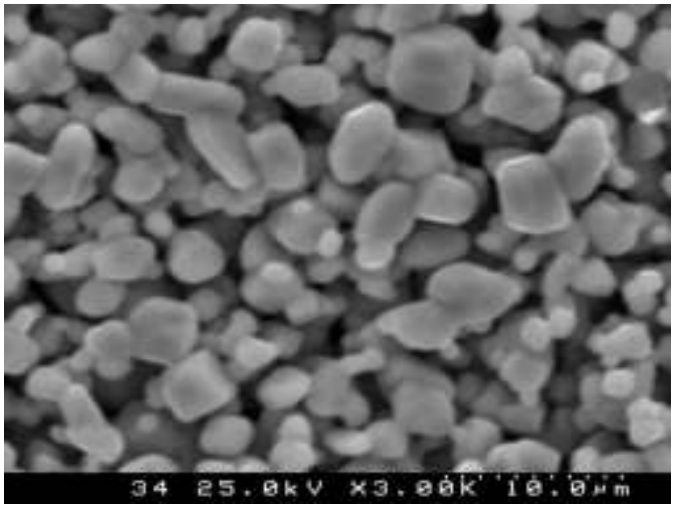


Figure 42. SEM surface micrograph of $Cu_3TeO_6$ sintered at 860$^{o}$C.

6.6.2 Dielectric properties of the $Cu_3TeO_6$ thick film

The relative dielectric permittivity of the $Cu_3TeO_6$ thick films sintered at 860$^{o}$C (Figure 43) were measured from 40 to 120$^{o}$C within the frequency range of 1 KHz and 1 MHz. Compared with bulk ceramics, the thick film has poor dielectric property, namely low dielectric permittivity. This can be attributed to the fact that the microstructure of film is less dense than its bulk ceramic counterpart. To improve the density and thus dielectric property of thick films,

two ways could be used: (1) reduce the particle size to the sub-nanometric range. (2) isostatic pressing before sintering, could increase the green density of the films and increase the final density.

Moreover, the temperature coefficient of the dielectric permittivity for the thick film sintered at 860°C are 9.5, 1.8, 1.5 and $6.3\times10^3$ ppm·°C$^{-1}$ when measured at frequency of 1 MHz, 100 kHz, 10 kHz and 1kHz, respectively.

The loss tangent (Figure 44) of $Cu_3TeO_6$ thick films seems to be influenced more significantly at low frequencies than at high frequencies. At 1 MHz, the loss tangent is almost not affected by the temperature and maintain a relatively small value, lower than 0.007.

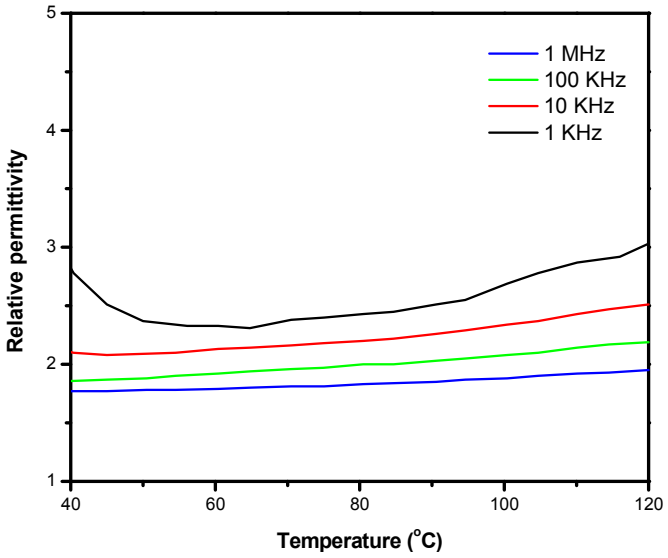


Figure 43. The temperature dependence of dielectric permittivity for $Cu_3TeO_6$ thick film sintered at 860°C. The measurements were done at 1 kHz, 10 kHz, 100 kHz and 1 MHz.

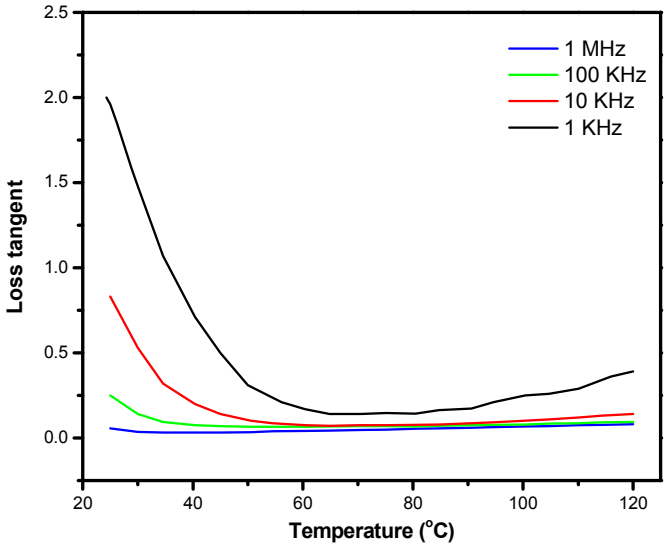


Figure 44. The loss tangent of $Cu_3TeO_6$ thick film sintered at 860°C. The measurements were done at 1 kHz, 10 kHz, 100kHz and 1 MHz.

In the precursor synthesis process, $Cu_3TeO_6$ and $CuTe_2O_5$ were obtained as monophasic compositions from the solid stated reactions of $3CuO+TeO_2$ and $CuO+2TeO_2$, respectively. The sintering behaviors of the $Cu_3TeO_6$ ceramics are determined from the profiles of volume shrinkage vs. temperature and relative density vs. temperature. $Cu_3TeO_6$ ceramic is well sintered at 865°C and shows a relative density of 93% as verified by the scanning electron microscopy (SEM) images. The dielectric permittivity is around 14 when measured at 100 kHz. The temperature coefficient of dielectric permittivity is extremely high, making the monophasic $Cu_3TeO_6$ ceramic not suitable for the LTCC technology. The thickness of green films increased nearly linearly with the applied voltage. The $Cu_3TeO_6$ thick film on platinized silicon is sintered at 860°C and no compositional change is detected. Sintering of the films on carbon-coated copper foil in air led to severe warpage of substrate and detachment of the films. The thick films have

poorer dielectric properties in comparison with bulk ceramics due to the difference in microstructure.

# Chapter 7

# Summary and future Work

## 7.1 Summary

(1) The phase formation of CuO-$TeO_2$ binary system was studied through the solid state reactions. Copper oxide (CuO) and tellurium dioxide ($TeO_2$) as starting materials with different stoichiometries were calcined at various temperatures. At 600$^{o}$C, the $CuTe_2O_5$ and $Cu_3TeO_6$ were obtained as mono-phasic compounds for the CuO+2$TeO_2$ and 3CuO+$TeO_2$ systems, respectively.

(2) Sintering of $Cu_3TeO_6$ ceramics was performed from 750$^{o}$C to 900$^{o}$C and the ceramics were characterized from the crystallographic, microstructural and electrical properties point of view. $Cu_3TeO_6$ ceramics are well sintered at 865$^{o}$C, possessing a relative density of 93% and volumetric shrinkage of 29%. Compositional change of the $Cu_3TeO_6$ phase was detected for the ceramics sintered at 900$^{o}$C, with namely the formation of CuO. The dielectric permittivity of the ceramics increased with sintering temperature. For dense $Cu_3TeO_6$ ceramics the dielectric permittivity at 1 MHz is 12.7. However, the loss tangent and the temperature coefficient of dielectric permittivity of the $Cu_3TeO_6$ ceramics are too high for their immediate applications in the LTCC technology. Strategies for the reduction of the dielectric losses and TC$\varepsilon_r$ are required.

(3) Fabrication of $Cu_3TeO_6$ thick films was carried out by the electrophoretic deposition (EPD) method. In this work, the acetone was used as suspension media while platinized silicon were used for the deposition. The thickness of the green films exhibited a linear relationship with the applied voltage, however, the quality of the films deteriorates for voltages higher than 300V. The influences of the deposition time is significant in the initial stage and declines as the deposition proceeds further.

(4) Sintering of the films was conducted: 800$^{o}$C, 820$^{o}$C, 840$^{o}$C and 860$^{o}$C. XRD analysis data shows that the chemical composition of $Cu_3TeO_6$ is stable throughout the sintering process. Films on the silicon substrates were well sintered at 860$^{o}$C. The relative dielectric permittivity of the films is lower than that of the bulk ceramics. This can be improve by reduction of the particle size of the starting materials and the isostatic pressing before sintering.

## 7.2 Future work

### 7.2.1 Phase formation of the CuO-$TeO_2$ system

Further systematic work is needed to exploit other compositions in the CuO-$TeO_2$ system, especially the phase formation of $CuO+2TeO_2$.

### 7.2.2 Tuning the dielectric properties of $Cu_3TeO_6$ ceramics

In this thesis, we investigated the sintering and properties of $Cu_3TeO_6$ ceramics as well as the fabrication of $Cu_3TeO_6$ thick films. The dielectric properties of the $Cu_3TeO_6$, however, did not meet the strict requirements for applications in LTCC technology, which require low dielectric losses and low temperature coefficient of the permittivity. Tuning the dielectric properties is crucial to the applications of $Cu_3TeO_6$ ceramics. For instance, the temperature coefficient of dielectric permittivity can be adjusted to a near-zero value by sintering $Cu_3TeO_6$ with a composition having a large negative TC$\varepsilon_r$.

### 7.2.3 Sintering of $Cu_3TeO_6$ thick films on copper substrates

Preventing the copper from oxidation at higher temperatures is a challenge. During the course of this work preliminary attempts were tried by using a carbon coating on the surfaces of the copper foil. These attempts were not particularly satisfactory so other strategies are required to achieve this goal.

# References


1. Dassow, S.V., *Low-firing and burnishing*. 2009, Ohio: American Ceramic Society.
2. M.A. Vartanyan, E.S.L., N. A. Popova, *Low firing temperature ceramic for microcircuit substrate.* Glass and Ceramics 2008. **65**: p. 27-30.
3. Rieldel, R., G. Passing, and H. Schonfelder, *Synthesis of the dense silicon-based ceramics at low temperatures.* Nature, 1992. **355**(6362): p. 714-717.
4. Takashi Hayashi, T.H., *Piezoelectric properties of low temperatre sintered PBMNZT ceramics with chemically added LiBiO2 sintering aid.* Journal of European Ceramic Society, 2005. **25**: p. 2437-2441.
5. Kwon, D.K., *Ultra-low temperature processing of barium tellurate dielectrics*, in *Department of Materials Science and Engineering*. 2006, Pennsylvania State University.
6. DW. Kim, C. K. Kim, C. S. Yoon, *Low-temperature sintering and microwave dielectric properties of Ba5NbO15-BaNb2O6 mixtures for LTCC applications.* Journal of the European Ceramic Society, 2003. **23**: p. 2597-2601.
7. Jantunen, H., et al., *Preparing low-loss low-temperature cofired ceramic material without glass addition* Journal of American Ceramic Society, 2000. **83**(11): p. 2855-2857.
8. Li, Q.Z., W. Li, and J. Shi, *A new microwave dielectric ceramic for LTCC applications.* Journal of European Ceramic Society, 2006. **89**(5): p. 1733-1735.
9. Haertling, G.H., *Ferroelectric ceramics: History and technology* Journal of American Ceramic Society, 1999. **82**: p. 797-818.
10. Muralt, P., *Ferroelectric thin films for micro-sensors anf actuators: a review.* Journal of Micromechanics and Microengineering, 2000. **10**: p. 136-146.
11. Nielsena, E.R., E. Ringgaarda, and M. Kosecb, *Liquid-phase sintering of $Pb(Zr,Ti)O_3$ using $PbO–WO_3$ additive* Journal of the European Ceramic Society, 2002. **22**: p. 1847-1855.
12. Hayashia, T., T. Inouea, and Y. Akiyamab, *Low temperature sintering of PZT powders coated with $Pb_5Ge_3O_{11}$ by sol–Gel method.* Journal of the European Ceramic Society, 1999. **19**: p. 999-1002.
13. Ngamjarurojana, A., S. Ural, and S.H. Park, *Piezoelectric properties of low temperature sintering in $Pb(Zr,Ti)O_3$-$Pb(Zr,Ti)_{1/3}Nb_{2/3}O_3$ ceramics for piezoeletric transformers applications.* Ceramics International, 2008. **34**: p. 705-708.
14. Zhu, Q. and B. Fan, *Low temperature sintering of 8YSZ electrolyte film for intermediate temperature solid oxide fuel cells* Solid State Ionics, 2005. **176**: p. 889-894.
15. Ji-Guang Li, T.I., Toshiyuki Mori, *Low temperature processing of dense samarium-doped CeO2 ceramics: sintering and grain growth behaviors.* Acta Materialia, 2004. **52**: p. 2221-2228.
16. K. Singh. S. A. Acharya, S.S.B., *Low temperature processing of dense samarium-doped CeO2 ceramics: sintering and intermediate temperature ionic conductivity.* Ionics, 2007. **13**(6): p. 429-434.
17. Muralidharan, P., S.H. Jo, and D.K. Kim, *Electrical Conductivity of Submicrometer Gadolinia-Doped Ceria Sintered at 1000 degrees C Using Precipitation-*

*Synthesized Nanocrystalline Powders.* Journal of American Ceramic Society, 2008. **91**(10): p. 3267-3274.
18. Birol, H., *Fabrication of low temperature co-fired ceramic (LTCC)-based sensor and micro-fluidic structures*. 2007, Ecole Politechnique Federale de Lausanne: Lausanne.
19. Yeung, L.K. and K.L. Wu, *A compact second-order LTCC bandpass filter with two finite transmission zeros.* IEEE transactions on microwave theory and techniques, 2003. **51**(2): p. 337-341.
20. Golonka, L.J., *Technology and applications of low temperature cofired ceramics based sensors and microsystems.* Bulletin of the Polish Academy of science, 2006. **54**(2): p. 221-231.
21. Matjaz Valant, D.S., *Glass-free low-temperature cofired ceramics: calcium germanates, tellurates and silicates.* Journal of the European ceramic society, 2004. **24**: p. 1715-1719.
22. Shimada, Y., K. Utsumi, and M. Suzuki, *Low firing temperature multilayer glass-ceramic substrate.* IEEE Transactions Components Hybrids Manufaction Technology, 1983. **6**(4): p. 382-388.
23. Randall, C.A., A. Kelnberger, and G.Y. Yang, *High strain piezoelectric multilayer actuators-a material science and engineering challenge.* Journal of Electroceramics, 2005. **14**: p. 177-191.
24. Udovic, M., M. Valant, and D. Suvrov, *Phase formation and dielectric characterization of the Bi2O3-TeO2 system prepared in an oxygen atomosphere.* Journal of American Ceramic Society, 2004. **87**(4): p. 591-597.
25. X.M. Chen, Y.H.S., X.H. Zheng, *High permittivity and low loss dielectric ceramics in the BaO-La2O3-TiO2-Ta2O5.* Journal of European Ceramic Society, 2003. **23**: p. 1571-1575.
26. Matters-Kammerer, M., U. Mackens, and K. Reimann, *Material properties and RF applications of high k and ferrite LTCC ceramics.* Microelectronics Reliability, 2006. **46**: p. 134-143.
27. Sebastian, M.T. and H. Jantunen, *Low loss dielectric materials for LTCC applications.* International Materials Review, 2008. **53**(2): p. 57-81.
28. Bian, J., D. Kim, and K.S. Hong, *Glass-free LTCC microwave dielectric ceramics* Materials Research Bulletin, 2005. **40**(12): p. 2120-2129.
29. Bau, H.H., J. Zhu, and S. Qian, *A magneto-hydrodynamically controlled fluidic network.* Sensors and Actuators B: Chemistry, 2003. **88**: p. 207-218.
30. Zhong, J., M. Yi, and H.H. Bau, *Magneto hydrodynamic pump fabricated with ceramic tapes.* Sensors and Actuators A, 2002. **96**: p. 59-66.
31. Fonseca, M.A., J.M. English, and M.v. Arx, *Wireless micro-machined ceramic pressure sensor for high-temperature applications.* Journal of Microelectromechanical Systems, 2002. **11**: p. 337-343.
32. Li, J. and G.K. Ananthasureth, *Three-dimensional low temperature co-fired ceramic shells for miniature system applications.* Journal of Micromechanics and Microengineering, 2002. **12**: p. 198-203.
33. Baker, A., M. Lanagan, and C. Randall, *Integration concepts for the fabrication of LTCC structures.* International Journal of Applied Ceramic Technology, 2005. **2**: p. 514-520.

34. Martinez-Cisneros, C.S., N. Ibenaz-Garcia, and F. Valdes, *LTCC microflow analyzer with monolithic integration of thermal control.* Sensors and Actuators, 2007. **A138**: p. 63-70.
35. El-Mallawany, R.A.H., *Tellurite Glasses Handbook*. 2002: CRC Press.
36. Feger, C.R., G.L. Schimek, and J.W. Kolis, *Hydrothermal synthesis and characterization of $M_2Te_3O_8$ (M=Mn,, Co, Ni, Cu, Zn): A series of compounds with the Spiroffite structure.* Journal of Solid State Chemistry, 1999. **143**.
37. Su, X., A. Wu, and P. M.Vilarinho, *Titanium tellurite thick films prepared by electrophoretic deposition and their dielectric properties.* Scripta Materialia, 2009. **61**: p. 536-539.
38. Yamada, T. and H. Iwasaki, *New ferroelectric compound $SrTeO_3$.* Applied Physics Letters, 1972. **21**(3): p. 89-90.
39. Yamanaka, S. and M. Miyake, *Study of the ternary Ti-Te-Osystem.* Journal of the Less Common Metals, 1990. **159**: p. 179-189.
40. Bindi, L. and C. Cipriani, *The crystal structure of Winstanleyite $TiTe_3O_8$ from the grand central mine, tombstone, Arizona.* The Canadian Mineralogist, 2003. **41**: p. 1469-1473.
41. Masaki Maeda, T.Y., Takuro Ikeda, *Dielectric charateristics of several complex oxide ceramics at microwave frequencies.* Japanese journal of applied physics, 1987. **26**(2): p. 76-79.
42. Udovic, M., M. Valant, and D. Suvrov, *Dielectric characterization of ceramics from the $TiO_2$-$TeO_2$ system.* Journal of the European Ceramic Society, 2001. **21**: p. 1735-1738.
43. Huang, C. and M. Weng, *Low-fire $BiTaO_4$ dielectric ceramics for microwave applications.* Materials Letters, 2000. **43**: p. 32-35.
44. Kagata, H., J. Kato, and I. Kameyama, *Low-fire bismuth-based dielectric ceramics for microwave use.* Japanese Journal of Applied Physics, 1992. **31**(9B): p. 3122-3155.
45. Foldvari, I., A. Peter, and L.A. Kappers, *Basic spectroscopic properties of bismuth tellurium oxide, Bi2TeO5.* Journal of Materials Science, 1992. **27**: p. 750-754.
46. Kikushi, T., Y. Kitami, and M. Yokoyama, *Pseudo-binary system $Bi_2O_3$-$TeO_3$ in air.* Journal of Materials Science, 1989. **24**: p. 4275-4278.
47. Udovic, M., M. Valant, and D. Suvrov, *Phase formation and dielectric properties of the $Bi_2O_3$-$TeO_2$ system prepared in an oxygen atomsphere.* Journal of American Ceramic Society, 2004. **87**(4): p. 591-597.
48. G. Subodh, M.T.S., *Glass-free $Zn_2Te_3O_8$ microwave ceramic for LTCC applications.* Journal of American Ceramic Society, 2007. **90**(7): p. 2266-2268.
49. Valant, M. and D. Suvorov, *Glass-free low-temperature co-fired ceramics: calcium germanates, silicates and tellurates.* Journal of the European Ceramic Society, 2004. **24**: p. 1715-1719.
50. Kwon, D.K., M.T. Lanagan, and T. Shrout, *Microwave dielectric properties of $BaO$-$TeO_2$ binary compounds.* Materials Letters, 2007. **61**: p. 1827-1831.
51. Jiao, X., C. Zhong, and S. Zhang, *Microwave dielectric properties of $BaO$-$TiO_2$-$TeO_2$ ternary system.* Journal of Materials Science, 2010. **45**: p. 3331-3335.
52. Kwon, D.K., M.T. Lanagan, and T.R. Shrout, *Synthesis of $BaTiTe_3O_9$ ceramics for LTCC application and its dielectric properties.* Journal of the Ceramic Society of Japan, 2005. **113**(3): p. 216-219.
53. Ayres, R.U. and L.W. Ayres, *A Handbook of Industrial Ecology*

2002, Cheltenham: Edward Elgar Publishing, Inc.
54. Hassan, M.A. and C.A. Hogarth, *A study of structural, electrical and optical properties of copper tellurium oxide glasses.* Journal of Materials Science, 1988(23): p. 2500-2504.
55. Hostachy, A. and J. Coing-boyat, *Structure crystalline de $Cu_3TeO_6$.* C. R. Seances Acad. Sci, Ser. B, 1968. **267**: p. 1435.
56. Falck, L. and O. Lindqvist, *Tricopper tellurate.* Acta Crystallografica, 1978. **B34**: p. 896-897.
57. Lindqvist, O., *On the structures of $CuTeO_3$ and $CuTe_2O_5$.* Acta Chemica Scandinavica, 1971. **25**(2): p. 740.
58. K.Hanke and V. Kupcik, *The crystal structure of $CuTe_2O_5$.* Acta Crystallografica, 1973. **B29**: p. 963-970.
59. Moret, J., E. Philippot, and M. Maurin, *Etude structurale de deux nouvelles phases cristallines $TeO_2$, $CuO$-$2TeO_2$, $CuO$.* Comptes Rendus de l'Académie des Sciences, 1969. **C269**: p. 123-125.
60. Lindqvist, O., *The crystal structure of $CuTeO_3$.* Acta Chemica Scandinavica, 1972. **26**: p. 1423-1430.
61. I. I. Ivanova, M.R.M., I. B. Dimitriev, Doklady Bolgarskoi akademii nauk, 1972. **25**: p. 1391.
62. Gospodinov, G.G., *Phase states of copper orthotellurates in an aqueous medium and thermolysis.* Journal of Materials Science Letters, 1992. **11**: p. 1460-1462.
63. Zhi Fu, P.M.V., A. Wu, A. I. Kingon, *Textured Microstructure and dielectric properties relationship of $BaNd_2Ti_5O_{14}$ thick films prepared by electrophoretic deposition.* Advanced functional materials, 2009(19): p. 1071-1081.
64. Fu, Z., A. Wu, and P.M. Vilarinho, *Low dielectric loss $BaNd_2Ti_5O_{14}$ thick films prepared by an electrophoretic deposition technique* Applied Physics Letters, 2007. **90**: p. 052912-052914.
65. Vilarinho, P.M., *Functional materials: properties, processing and applicaitons*, in *Scanning Probe Microscopy: Characterization, Nanofabrication and Device Applications of Functional Materials*, P.M.V.*e. al*., Editor. 2005, Kluwer Academic Publishers. p. 3-33.
66. *Handbook of thin film process technology*, ed. S.I.S. D. A. Glocker. 1995, Bristol.
67. Zhou, Q.F., H.L.W. Chan, and C.L. Choy, *PZT ceramic/ceramic 0-3nanocomposite films for ultrasonic transducer applications.* Thin Solid Films, 2000. **375**: p. 95-99.
68. M.R. Gonga-Rubio, P.E.-V., L. Sola-Laguna, *Overview of low temperature co-fired ceramics tape technology for meso-system technology.* Sensors and actuators, 2001(A24): p. 222-241.
69. Altenburg, H., J. Plewa, and G. Plesch, *Thick films of ceramic, superconducting, electroceramic materials.* Pure and Applied Chemistry, 2002. **74**(11): p. 2083-2096.
70. Dorey, R.A. and R.W. Whartmore, *Electroceramic thick films fabrication for MEMS.* Journal of Electroceramics, 2004(12): p. 19-32.
71. Solis, J., S. Saukko, and L. Kish, *Semiconductor gas sensors based on nanostructured tungsten oxide*
Thin Solid Films, 2001. **391**(2): p. 255-260.
72. Izu, N., W. Shin, and N. Murayarna, *Resistive oxygen gas sensors based on $CeO_2$ fine powder prepared using mist pyrolysis.* Sensors and Actuators B: Chemical, 2002. **87**(1): p. 95-98.

73. Martinelli, G., M.C. Carotta, and M. Ferroni, *Screen-printed perovskite-type thick films as gas sensors for environmental monitoring.* Sensors and Actuators B: Chemical, 1999. **55**(2-3): p. 99-110.
74. Krebs, F., *Fabrication and processing of polymer solar cells: a review of printing and coating techniques.* Solar Energy Materials and Solar Cells, 2009. **93**: p. 394-412.
75. Hotza, D. and P. Greil, *Review: aqueous tape casting.* Materials Science and Engineering, 1995. **A202**: p. 206-217.
76. Annika Kristoffersson, E.C., *Tape casting of alumina in water with an acrylic latex binder.* Journal of European Ceramic Society, 1997(17): p. 289-297.
77. Mistler, R.E., *Tape casting,* , in *Engineering materials handbook, Volume 4, Ceramics and glasses*. 1991, ASM International. p. 161-165.
78. Kristoffersson, A. and E. Carlstrom, *Tape casting of alumina in water with an acrylic latex binder* Journal of the European Ceramic Society, 1997. **17**: p. 289-297.
79. R.L. Callender, C.J.H., N. M. Shapiro, *Aqueous synthesis of water-soluble alumoxanes: Environmentally benign precursors to alumina and aluminum-based ceramics* Chemistry of materials, 1997. **9**: p. 2418-2433.
80. Calvert, P., *Ink-jet printing for materials and devices.* Chemistry of Materials, 2001. **13**: p. 3299-3305.
81. Glowacki, B.A., *Preparation of $Bi_2Sr_2CaCu_2O_8$-x tracks and thick films by jet printing.* Superconductor Science and Technology Impact Factor, 2000. **13**: p. 584-591.
82. Sarkar, P. and P.S. Nicholson, *Electrophoretic deposition (EPD): mechanisms, kinetics and applications to ceramics.* Journal of American Ceramic Society, 1996. **79**(8): p. 1987-2002.
83. Laxmidhar Besra, M.L., *A review on fundamentals and applications of Electrophoretic deposition(EPD).* Progress in Materials Science, 2007(52): p. 1-61.
84. Tassel, J.V. and C. Randall, *Mechanisms of electrophoretic deposition.* Key Engineering Materials, 2006. **314**: p. 167-173.
85. Zhitomirosky, I., *Cathodic electrodeposition of ceramic and organoceramic materials. Fundamental aspects* Advances in Colloid and Interface Science, 2002. **97**: p. 277-315.
86. LJ, Z., XQ Huang, RB, Zhu, *Optimization on technical parameters for fabrication of SDC film by screen-printing used as electrolyte in IT-SOFC* Journal of physics and chemistry, 2008. **69**: p. 2019-2024.
87. Ishihara, T., K. Sato, and Y. Mizuhara, *preparation of yttria-stabilized zirconia (YSZ) films for a solid oxide fuel cells by electrophoretic deposition.* Chemistry Letters, 1992(6): p. 943-946.
88. Corni, I., M.P. Ryan, and A.R. Boccaccini, *Electrophoretic deposition: From traditional ceramics to nanotechnology* Journal of the European Ceramic Society, 2008. **28**(7): p. 1353-1367.
89. Biest, O.V.d. and L. Vandeperre, *Electrophoretic deposition of materials.* Annual Review of Materials Science, 1999. **29**: p. 327-352.
90. Lyklema, J., *Principles of the stability of lyophobic colloidal dispersions in the non-aqueous media.* Advances in Colloid and Interface Science 1968. **2**: p. 65-114.

91. Ishihara T, S.K., Kudo T, Nishiguchi H, Akbay T, Tahika Y, *Preparation of Yttrian-stabilized zirconia thin films on strontium doped $LaMnO_3$ cathode substrate via electrophoretic deposition for solid oxide fuel cells.* Journal of American Ceramic Society, 2000. **83**(8): p. 1921-1927.
92. Borgwardt, R. and K. Bruce, *Effect of specific area on the reactivity of CaO with $SO_2$.* Aiche Journal, 1986. **32**: p. 239-246.
93. Rodrigues, A.C.M., R. Keding, and C. Ruessel, *Mixed former effect between $TeO_2$ and $SiO_2$ in the $Li_2O{\cdot}TeO_2{\cdot}SiO_2$ system* Journal of Non-Crystalline Solids, 2000. **273**: p. 53-58.
94. D.K. Kwon, M.T.L. and T. Shrout, *Microwave dielectric properties of BaO-TeO2 binary compounds.* Materials Letters, 2007. **61**: p. 1827-1831.